






Simultaneous CAS9 editing of cpSRP43, LHCA6, and LHCA7 in *Picochlorum celeri* lowers chlorophyll levels and improves biomass productivity

Anagha Krishnan¹  | Melissa Cano¹ | Devin A. Karns¹  | Tyson A. Burch¹ | Maria Likhogrud² | Moena Aqui³ | Shaun Bailey³ | John Verruto³ | William Lambert³ | Fedor Kuzminov³ | Mahva Naghipor³ | Yingjun Wang³ | Christopher C. Ebmeier⁴  | Joseph C. Weissman²  | Matthew C. Posewitz¹ 

¹Department of Chemistry, Colorado School of Mines, Golden, Colorado, USA

²ExxonMobil Technology and Engineering Company, Annandale, New Jersey, USA

³Viridos, La Jolla, California, USA

⁴Department of Chemistry and Biochemistry, University of Colorado, Boulder, Colorado, USA

Correspondence

Anagha Krishnan and Matthew C. Posewitz, Department of Chemistry, Colorado School of Mines, Golden, CO 80401, USA.

Email: akrishnan@mines.edu and mposewit@mines.edu

Joseph C. Weissman, ExxonMobil Technology and Engineering Company, Annandale, New Jersey, USA.

Email: jcweissm@gmail.com

Funding information

ExxonMobil Technology and Engineering Company, United States

Abstract

High cellular pigment levels in dense microalgal cultures contribute to excess light absorption. To improve photosynthetic yields in the marine microalga *Picochlorum celeri*, CAS9 gene editing was used to target the molecular chaperone cpSRP43. Depigmented strains (>50% lower chlorophyll) were generated, with proteomics showing attenuated levels of most light harvesting complex (LHC) proteins. Gene editing generated two types of cpSRP43 transformants with distinct lower pigment phenotypes: (i) a transformant ($\Delta srp43$) with both cpSRP43 diploid alleles modified to encode non-functional polypeptides and (ii) a transformant (STR30309) with a 3 nt in-frame insertion in one allele at the CAS9 cut site (non-functional second allele), leading to expression of a modified cpSRP43. STR30309 has more chlorophyll than $\Delta srp43$ but substantially less than wild type. To further decrease light absorption by photosystem I in STR30309, CAS9 editing was used to stack in disruptions of both LHCA6 and LHCA7 to generate STR30843, which has higher (5–24%) productivities relative to wild type in solar-simulating bioreactors. Maximal productivities required frequent partial harvests throughout the day. For STR30843, exemplary diel bioreactor yields of $\sim 50 \text{ g m}^{-2} \text{ day}^{-1}$ were attained. Our results demonstrate diel productivity gains in *P. celeri* by lowering pigment levels.

KEYWORDS

biomass productivity, CAS9 editing, cpSRP43, photosynthetic efficiency, *Picochlorum celeri*

1 | INTRODUCTION

Microalgae are able to efficiently convert sunlight into biomass (stored chemical energy), which can be used in a variety of sustainable

biotechnological applications including food security, sustainable aviation fuels, nutraceuticals, and renewable biopolymers (Davis et al., 2011; Gimpel et al., 2013; LaPanse et al., 2021; Schenk et al., 2008; Sheehan et al., 1998). Importantly, some microalgae thrive in saline water and can

This is an open access article under the terms of the [Creative Commons Attribution-NonCommercial-NoDerivs](https://creativecommons.org/licenses/by-nc-nd/4.0/) License, which permits use and distribution in any medium, provided the original work is properly cited, the use is non-commercial and no modifications or adaptations are made.

© 2023 The Authors. *Plant Direct* published by American Society of Plant Biologists and the Society for Experimental Biology and John Wiley & Sons Ltd.

be grown using marginal lands/marshes/offshore sites, which make these saltwater photoautotrophs attractive complements, and potential alternatives, to land-based feedstocks that have substantial freshwater demands (Benedetti et al., 2018; Dismukes et al., 2008). The full realization of the potential of microalgae is currently limited by production costs, which will benefit from biomass productivity improvements.

While theoretical solar-to-biomass conversion efficiency estimates of 8–10% (18–22% PAR→ biomass) are calculated to yield 77–100 g m⁻² day⁻¹, the best sustained productivities of outdoor dense algal cultures are in the range of 20–35 g m⁻² day⁻¹ translating to an ~3% conversion efficiency (Grobbelaar, 2000; Lee, 2001; Melis, 2009; Moheimani & Borowitzka, 2007; Sheehan et al., 1998; Weissman & Nielsen, 2016). The “low-light” acclimated state of microalgae with high pigment content in dense-mass cultures is a primary contributor to this inefficiency (Grobbelaar, 2010; Grobbelaar et al., 1995; Kirst et al., 2017; Melis, 2009; Weissman, 1978; Weissman & Nielsen, 2016). Here, individual cells compete for light by maximizing their peripheral light harvesting antenna to increase their ability to capture photons in light-limited environments. High optical cross sections lead to saturation of the photosynthetic apparatus with the consequence that many absorbed photons are dissipated by non-photochemical routes leading to reduced photosynthetic efficiency. One proposed solution is to develop strains with lower pigment levels (Cazzaniga et al., 2014; Dabes et al., 1970; Formighieri et al., 2012; Jeong et al., 2017; Kirst, Garcia-Cerdan, Zurbriggen, Ruehle & Melis, 2012; Kirst et al., 2014; Kwon et al., 2013; Melis et al., 1998; Musgnug et al., 2007; Nakajima & Ueda, 2000; Negi et al., 2020; Oey et al., 2013; Perin et al., 2015; Perrine et al., 2012; Polle et al., 2003; Radmer & Kok, 1977). In principle, depigmentation will reduce light absorption by individual cells enabling more cells to photosynthesize, contributing towards culture productivity. Multiple strategies have been used to manipulate light harvesting antenna sizes and generate depigmented algae including but not limited to *Chlamydomonas*, *Dunaliella*, *Nannochloropsis*, *Chlorella*, *Phaeodactylum*, and cyanobacteria. Almost all had lower chlorophyll content, smaller peripheral antenna, and used high light more effectively (Huesemann et al., 2009; Jeong et al., 2017; Kirst, Garcia-Cerdan, Zurbriggen & Melis, 2012; Kirst, Garcia-Cerdan, Zurbriggen, Ruehle & Melis, 2012; Musgnug et al., 2007; Nymark et al., 2019; Perrine et al., 2012; Polle et al., 2000, 2003) (Baek et al., 2016; Beckmann et al., 2009; Cazzaniga et al., 2014; Kirst et al., 2014; Nakajima et al., 2001; Negi et al., 2020; Perin et al., 2015). However, only a few of them demonstrated successful improvements in productivity/growth in mass culture (Cazzaniga et al., 2014; Nakajima et al., 2001; Negi et al., 2020; Perin et al., 2015).

Here, we describe depigmented strains of a remarkably fast-growing, high-light tolerant microalga, *Picochlorum celeri*. The *Picochlorum* genus (Henley et al., 2004) has become the focus of several recent studies because of their high stress tolerances, as well as their small, compact genomes (Barten et al., 2020; Dahlin et al., 2019; Foflonker et al., 2016; Gonzalez-Esquer et al., 2019; Manjre et al., 2022; Weissman et al., 2018). *P. celeri* demonstrates broad halotolerance, an exceptional ability to thrive at high light intensities (>2000 μmol photons m⁻² s⁻¹), temperatures (>35°C), and salinities (2–3× seawater), and can attain rapid doubling times of ~2 h under optimal conditions

(Krishnan et al., 2021). Recently, *P. celeri* demonstrated among the highest monthly productivity (~36 g m⁻² day⁻¹) reported to-date for a marine alga in an outdoor field trial at the Arizona Center for Algae Technology and Innovation testbed (Krishnan et al., 2021).

P. celeri's chlorophyll content is very responsive to irradiance, becoming relatively low (~1.2% of ash-free-dry-weight [AFDW]) at high irradiance (~2000-μmol photons m⁻² s⁻¹) and almost tripling at low light (60 μmol photons m⁻² s⁻¹) and diel culturing (~4.5% of AFDW) (Weissman et al., 2018). Because of the ability of *P. celeri* to develop a “low-light acclimated” physiology with high chlorophyll content, it is likely necessary to engineer a strain that remains in a more “high-light acclimated” state with less photosynthetic pigment content even in dense culture to improve solar-to-biomass conversion efficiencies.

Photosynthetic machinery in oxygenic phototrophs is composed of (i) two coupled, light-driven reaction centers, photosystem II (PSII) and photosystem I (PSI), involved in water splitting and the generation of low-potential electrons and (ii) peripheral light harvesting pigment-protein antenna complexes (LHCs), associated with each photosystem that are predominantly involved in the absorption of photons and transfer of energy to the respective reaction centers. In higher plants and microalgae, there are distinct LHC proteins, called light harvesting proteins of photosystem I (LHCA) and light harvesting proteins of photosystem II (LHCB), associated with PSI and PSII, respectively (Jansson et al., 1992; Grossman et al., 1995). All the LHCs are nuclear encoded and post-translationally imported to the chloroplast envelope where they are guided to the thylakoid membrane using the chloroplast signal recognition particle 43 (cpSRP) pathway. cpSRP43 and cpSRP54 form a soluble transit complex by binding to the hydrophobic LHCPs that traverses the stroma and docks to the thylakoid membrane by the interaction with cpFTSY and then ALB3 insertase (Kirst et al., 2014; Ziehe et al., 2018). In both microalgae and higher plants, cpSRP43, a molecular chaperone, plays a central role in LHCP recognition and in preventing misfolding of the incoming LHCPs (Falk & Sinning, 2010). Δ *srp43* mutants have been shown to display considerable decreases in the LHC pigment-protein complexes and have therefore been used as targets for engineering “truncated peripheral-antenna” mutants (Amin et al., 1999; Kirst, Garcia-Cerdan, Zurbriggen, Ruehle & Melis, 2012; Kirst et al., 2014; Kirst et al., 2018; Klimyuk et al., 1999).

Here, we apply CAS9 technology to edit cpSRP43 to lower pigment levels in the biotechnologically relevant alga *P. celeri* and further stack two LHCP polypeptide deletions into an edited cpSRP43 strain to better balance light capture between PSI and PSII and enable increased photosynthetic efficiencies. Lastly, we explore the effects of harvesting frequency in bioreactors to modulate biomass and pigment levels to improve biomass productivities.

2 | RESULTS

2.1 | *P. celeri* cpSRP43 molecular structure, guide design, and mutant generation

CpSRP43 is a multidomain protein composed of (i) ankyrin (ANK) repeats involved in the recognition and binding of LHCs; and

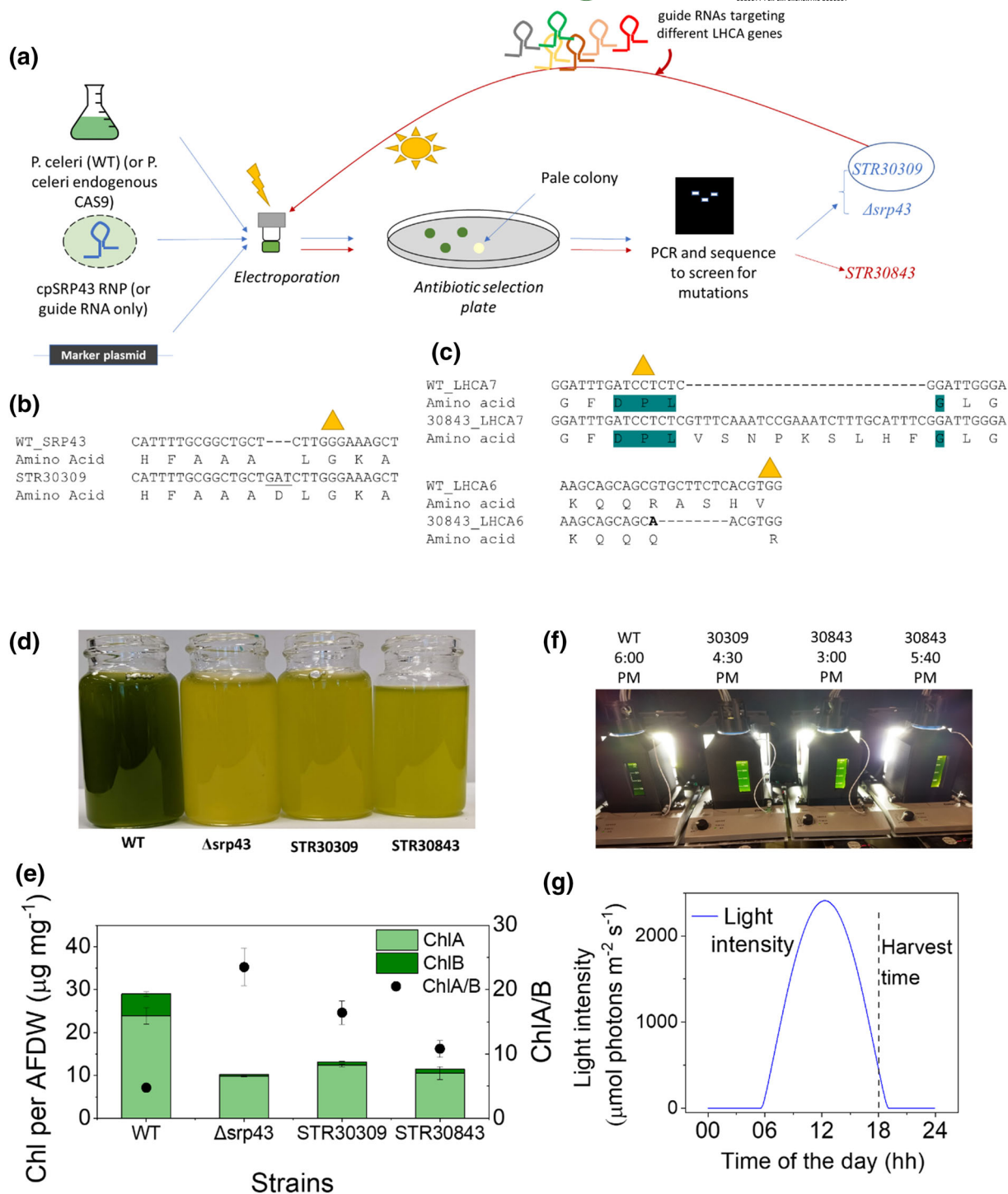


FIGURE 1 Screening and analysis cpSRP43 transformants: (a) schematic representation of cpSRP43 transformation protocol. (b) DNA sequencing of the cpSRP43 PCR fragment from STR30309. PAM motif is denoted by a triangle. Inserted nucleotides are underlined. Translated protein sequence is given below the DNA sequence. (c) DNA sequences of LHCA7 PCR fragment from STR30309 and STR30843. PAM motif is denoted by a triangle. Inserted nucleotides are underlined. Translated protein sequence is given below the DNA sequence. DPLG motif is highlighted in green. (d, e) Phenotype and chlorophyll content of wild type (WT), $\Delta srp43$, STR30309, and STR30843 in shake flask cultures grown in constant light, 1% CO₂ and 33°C. Each data point represents the average and standard deviation of two biological replicates. (f) ALGiSIM stations: Bottle 1: WT at 6 p.m. (1 h before sunset), Bottle 2: STR30309 at 4:30 p.m. (2.5 h before sunset), Bottle 3: STR30843 at 3 p.m., and Bottle 4: STR30843 at 5:40 p.m. (g) Light profile applied to the cultures and the harvest time point.

(ii) chromodomains (CD), which bind to the remaining polypeptides of the cpSRP pathway. The ANK domain of cpSRP43 binds to a highly conserved 18-amino acid region in the LHCs of both photosystems called the L18 loop, which contains a DPLG (Asp-Pro-Leu-Gly) signature motif (Stengel et al., 2008). Recognition of the DPLG motif by cpSRP43 is essential for the formation of a productive cpSRP43-LHC transit complex (Stengel et al., 2008). Using *Arabidopsis* cpSRP43 as a reference (Stengel et al., 2008), a homology model (Schwede et al., 2003) for *P. celeris* cpSRP43 was developed and the putative L18 binding location identified (Figure S1A). CAS9 guides were designed in the ANK motif close to the putative L18 binding site to abolish/alter cpSRP43-LHC binding (Figures S1A and 1b). The guide, in tandem with a marker plasmid, was electroporated into either wild type (WT) *P. celeris* using CAS9-RNP techniques (Krishnan et al., 2020) or into a *P. celeris* strain constitutively expressing CAS9 (Figure 1a). From the colonies that survived the antibiotic selection, several pale green candidates (low chlorophyll by visual examination), as well as a few dark colored colonies (likely edited in only one allele), were patched onto fresh plates. These transformants were examined for edits in the cpSRP43 gene by PCR amplification of the genomic cpSRP43 locus and amplicon sequencing.

Because *P. celeris* is a diploid organism with two genomic alleles, three distinct types of mutants were selected from the transformation (Figure 1): (i) both cpSRP43 coding alleles edited putatively resulting in complete loss of function (Δ srp43) strains; (ii) one allele intact (unedited) and the second allele disrupted (SRP43HET) (Figure S2); and (iii) one allele likely disrupted (no WT band detected by PCR under our amplification conditions), and the second allele having a 3 nucleotide insertion (in-frame edit) at the cut site resulting in a modified form of cpSRP43 protein with an additional amino acid inserted into the coding sequence (STR30309) (Figure 1). Heterozygous transformants (SRP43HET) did not have detectable pigment phenotypes under the conditions used in this study and were not pursued further (Figure S2). The Δ srp43 strain selected for detailed study here had the antibiotic selection marker inserted at the cut site of both genomic alleles. STR30309 has a 3-nucleotide (GAT) insertion at the CAS9 cut site in one allele resulting in an aspartic acid residue insertion as the 165th

amino acid located in the ANK1 binding domain (Figure S1B). Δ srp43 and STR30309 were highly depigmented demonstrating large (~2- to 3-fold) decreases in pigment content when grown as shake-flask batch cultures exposed to constant illumination of 600–800 μ mol photons $m^{-2} s^{-1}$ (Figure 1d,e).

To further decrease PSI light absorption, STR30309 was additionally modified using CAS9 to disrupt genes encoding LHCA polypeptides using a multiplexed approach where transformations were done in the presence of multiple LHCA guide RNAs targeting 6 different LHCA. Transformants with different combinations of LHCA genes modified were obtained, one of which (STR30843) had favorable photosynthetic phenotypes in preliminary studies and was selected for further characterizations. STR30843 has one modified allele of cpSRP43 (the other allele cannot be detected by PCR and is putatively non-functional, as observed in the parent STR30309 strain) and both alleles of LHCA6 and LHCA7 disrupted (Figure 1c–e). Interestingly, relative to STR30309, the stacked transformant STR30843 had more total chlorophyll under the diel culturing conditions tested (Table 1) despite the removal of two additional LHCA polypeptides. It is likely that a regulatory circuit in STR30843 is able to further modulate pigment levels in this heavily modified transformant.

2.2 | Single daily dilution

2.2.1 | Biomass productivities in diel light, dense-culture cultivation

To evaluate pigment levels and strain productivities in dense, diel cultures depigmented strains were grown in a custom-built, automated photobioreactor (ALGiSIM) that mimics outdoor pond environments (Figure 1) (Cano et al., 2021). Briefly, ALGiSIM uses four 400-ml-square bottle-culture vessels mounted on magnetic stir plates. Each bottle is illuminated by an LED panel from one side while the remaining three sides are covered by a black jacket to prevent stray light input. For semicontinuous operation (once daily dilution), a portion of

TABLE 1 Growth in the ALGiSIM at a dilution rate of 60% (single dilution) per day.

Parameters	WT	Δ srp43	STR30309	STR30843 (average)
Productivity ($g m^{-2} day^{-1}$)	43.2 (.6)	41.4 (.8)	43.7 (.6)	47.1 (1.1)
PAR-to-biomass conversion efficiency	6.4% (.1%)	6.2% (.1%)	6.5% (.1%)	7.0% (.1%)
Average specific growth rate (day^{-1})	.92 (.01)	.92 (.01)	.92 (.01)	.92 (.01)
Total chlorophyll ($mg L^{-1}$)	48.6 (.4)	18.1 (.35)	21.0 (.2)	24.3 (.4)
Chl/AFDW %	4.5 (.1)	1.8 (.1)	1.9 (.1)	2.1 (.1)
Chl a ($mg L^{-1}$)	39.7 (.3)	17.1 (.3)	18.9 (.2)	21.6 (.3)
Chl b ($mg L^{-1}$)	8.85 (.2)	1.00 (.1)	2.29 (.1)	2.73 (.08)
Chl a/Chl b	4.5 (.1)	17.6 (1.3)	8.3 (.2)	8.0 (.3)
AFDW ($g L^{-1}$)	1.10 (.01)	1.03 (.01)	1.10 (.01)	1.17 (.01)

Note: Each datapoint is the average and the standard error (given in the brackets) for 8-daily replicates. For STR30843, data represent the average and standard error for two separate bioreactor runs with 8-daily replicates sampled for each run.

Abbreviations: AFDW, ash-free-dry-weight; PAR, photosynthetically active radiation; WT, wild type.



the 400-ml culture volume is automatically harvested each day and replaced with fresh media using software-controlled liquid pumps. The remaining culture volume is inoculum for the next diel light period, whereas the harvested culture is biochemically analyzed as described below. Thus, cultures start at lower pigment/biomass density at dawn and gradually become denser through the light period.

WT, STR30843, STR30309, and $\Delta srp43$ were cultivated in the ALGiSIM, under diel conditions, at pH 6.9–7.2 (continuous bubbling with 2.25% CO₂) and a constant temperature of 33°C. Once per day, 60% of the cultures were harvested 1 h before sunset in the insolation profile shown in Figure 1g and the harvest volume replaced with fresh media. The typical growth profile in a daily culturing campaign is shown in Figure S3. The growth rate of the culture, on average, is determined by the dilution rate.

All three mutants were able to sustain a 60% daily dilution without being washed out, which is equivalent to an average specific growth rate of .92 day⁻¹. Mutant strains remained highly depigmented even during dense culture cultivation. $\Delta srp43$, STR30309, and STR30843 displayed >2-fold lower chlorophyll/AFDW as compared with the WT. WT had a chlorophyll content of 4.5 ± .1% of AFDW, whereas $\Delta srp43$, STR30309, and STR30843 had chlorophyll contents of 1.8 ± .1%, 1.9 ± .1%, and 2.1 ± .1% of AFDW, respectively. The chlorophyll density (mg L⁻¹) attained at harvest was also >2-fold lower in the mutants relative to WT (48.6 ± .4 mg L⁻¹ [Table 1]). Specifically, $\Delta srp43$ had the lowest chlorophyll concentration (18.1 ± .4 mg L⁻¹) followed by STR30309 (21.0 ± .2 mg L⁻¹) and STR30843 (24.3 ± .4 mg L⁻¹). The Chl a/b ratio in the WT, STR30843, STR30309, and $\Delta srp43$ were 4.5 ± .1, 8.0 ± .3, 8.3 ± .2, and 17.6 ± 1.3, respectively. In STR30309 and STR30843, the Chl a/AFDW is ~50% of the WT, whereas Chl b content dropped to 25% of WT levels. In $\Delta srp43$, Chl a/AFDW is ~45% of the WT, whereas Chl b decreased to ~13% of the WT.

The biomass density attained at the time of dilution was the highest in STR30843 (1.17 ± .01 g L⁻¹, *p* value < .005), whereas $\Delta srp43$ had a lower biomass density (1.03 ± .01 g L⁻¹, *p* value < .005) as compared with the WT and STR30309 (1.10 ± .01 g L⁻¹). Areal productivities determined from the daily volumetric productivity were not significantly different between WT (43.2 ± .6 g m⁻² day⁻¹) and STR30309 (43.7 ± .6 g m⁻² day⁻¹) (*p* value = .51), each having a light-to-biomass conversion efficiency of ~6.5% (photosynthetically active radiation [PAR]). STR30843 had productivities of 45.7 ± .9 g m⁻² day⁻¹ (*p* value w.r.t WT = .034) and 48.4 ± .7 g m⁻² day⁻¹ (*p* value w.r.t WT < .001) in the two different stations, with an average of 47.1 ± 1.1 g m⁻² day⁻¹ corresponding to 5–10% increase in biomass productivity compared with the WT. The $\Delta srp43$ strain had a slightly lower (statistically not significant) average productivity of 41.4 ± .8 g m⁻² day⁻¹ (*p* value w.r.t WT = .09). One-way analysis of variance (ANOVA) showed that STR30843 productivity was significantly higher than all other strains. STR30843 had a slightly higher PAR-to-biomass conversion efficiency of 7 ± .1% (*p* value w.r.t WT = .001), whereas $\Delta srp43$ was 6.2 ± .1% (*p* value w.r.t WT = .1).

Carotenoids in each strain were quantified using high-performance liquid chromatography (HPLC) (Figure 2a) (Cano

et al., 2021). Lutein, β -carotene, and neoxanthin were the major carotenoids, and violaxanthin, antheraxanthin, zeaxanthin, and canthaxanthin were detected at lower levels. On an AFDW basis, carotenoids were 1.2 ± .1% of biomass in the WT (~26% of all pigments), and the mutants demonstrated a 30% lower content (~7–8%/AFDW) but a higher percentage of all pigments (~38–45%). The decrease in absolute carotenoid levels came from a >3-fold lower neoxanthin (.12%/AFDW in the WT vs. ~.03–.04%/AFDW in the mutants) and ~1.4–1.7-fold reduction in the lutein content (.6%/AFDW in the WT vs. ~.4%/AFDW in the mutants). Xanthophylls, neoxanthin, and lutein are typically found in association with LHCs (Qin et al., 2015; Su et al., 2017).

In sum, all three mutants tested were highly depigmented demonstrating 50–55% decrease in pigment (chlorophyll and carotenoid) levels/AFDW even under diel-dense cultivation and were able to sustain a single 60% daily dilution regime. Furthermore, the modified SRP43 strain with an in-frame amino acid insert (STR30309) had features distinct from the $\Delta srp43$ deletion strain. In particular, the large change in the Chl a/b ratio between the strains suggest a loss of peripheral light harvesting antenna (“truncated antenna” phenotype) in the $\Delta srp43$ that is partially rescued in STR30309. Finally, STR30843 with the additional editing of genes encoding LHCA6 and LHCA7 in the STR30309 background displayed greater biomass productivities.

2.2.2 | Photophysiology of diel growth

To investigate the association of the light-harvesting antenna proteins and pigments with the two photosystems under diel conditions, 77-K chlorophyll fluorescence emission spectra were measured. Samples harvested from the ALGiSIM were diluted to a chlorophyll concentration of 5 μ g ml⁻¹, dark adapted for 10 min, flash frozen in liquid nitrogen and used for measurements. Excitation wavelength for the spectral analysis was set to 440 nm, and emission was measured between 650 and 800 nm (Figure 2b). Similar to *Chlamydomonas*, 77-K fluorescence emission spectrum of the WT is characterized by four distinct peaks: two major peaks at 685 nm (attributed to CP43/CP47) and 695 nm (CP47), a shoulder at 680 nm (representing LHCII), and a broad peak at ~708 nm (originating from PSI core and LHCI antenna). Emission spectra were normalized to the fluorescence at 685 nm (F685) (Lamb et al., 2018).

$\Delta srp43$, STR30309, and STR30843 displayed a lower relative LHCII fluorescence yield (F680) compared with WT (Figure 2b inset). This is consistent with a higher Chl a/b ratio suggesting a depletion of LHCII antenna pigment-protein complexes in the mutants. WT has a distinct 708-nm peak not observed in the mutants indicating an alteration either in the levels of PSI-LHCI, or the association between PSI and LHCI, in the mutants. When comparing across mutants, fluorescence yield from F708 (relative to F685) was the highest in $\Delta srp43$ followed by STR30309 and then STR30843 suggesting that STR30843 had the lowest amount of PSI-LHCI (relative to F685). Interestingly, the fluorescence emission at 695 nm (attributed to CP47) was higher in the

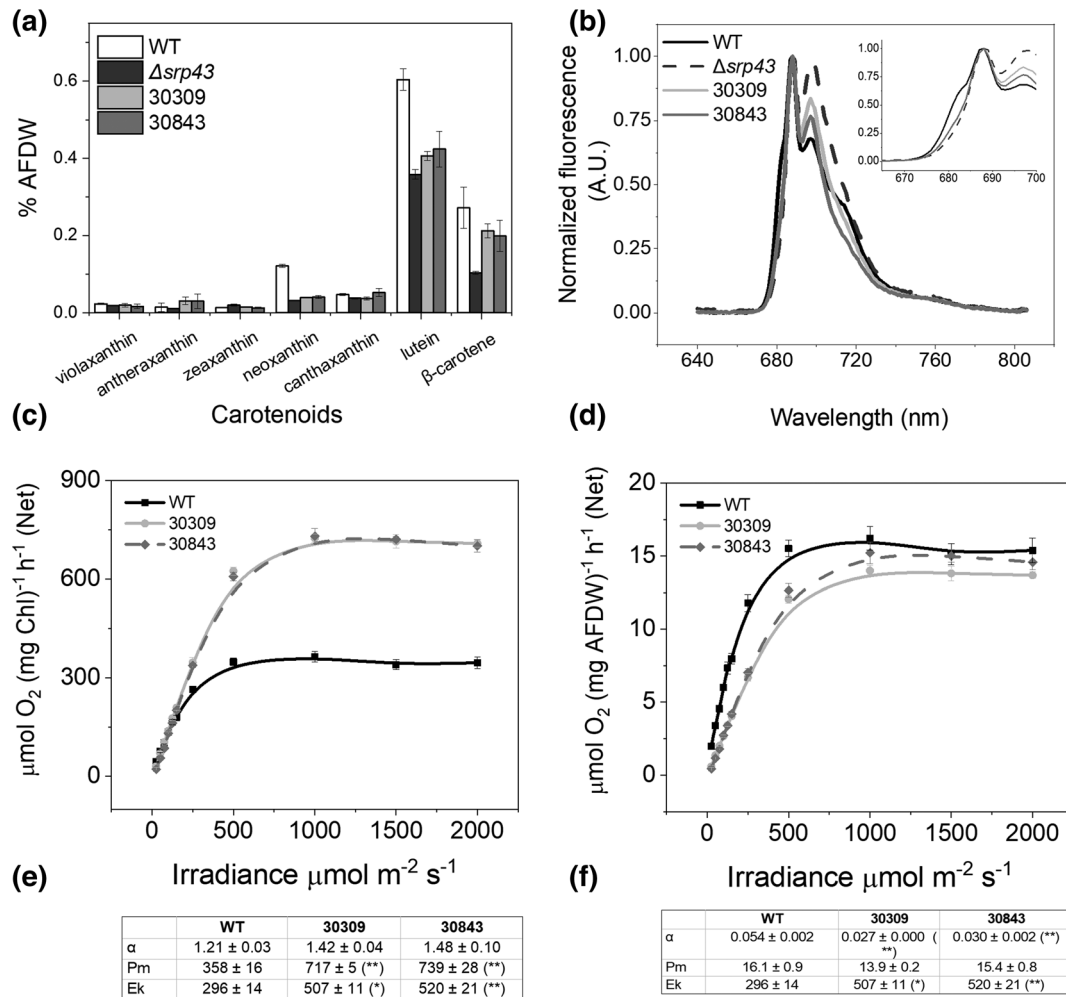


FIGURE 2 Photosynthetic characterization: (a) Abundance of individual carotenoids. Each data point represents the average and standard error for 4 daily replicates. (b) 77-K fluorescence emission spectra of *Picochlorum celeri* wild type (WT, black), STR30309 (light gray), and STR30843 (dark gray). Fluorescence emission spectra (440-nm excitation) were recorded for whole cells diluted to $5 \mu\text{g ml}^{-1}$ chlorophyll and flash frozen in liquid nitrogen. Traces have been normalized to F685 peak. Inset shows relative loss of the 680-nm peak in the mutants as compared with the WT. (c, d) Photosynthesis-Irradiance (P-I) curves and calculated parameters for *Picochlorum celeri* WT, STR30309, and STR30843 normalized to total chlorophyll (c, e) or ash-free-dry-weight (AFDW) (d, f). Data represent average and standard error of the net oxygen evolution rate for 4 daily replicates. Chlorophyll density of the suspension for the P-I experiment was $\sim 6\text{--}7 \mu\text{g ml}^{-1}$. WT, 30309, and 30843 were diluted 75, 37.5-fold, and 37.5-fold, respectively. Parameters given in (e) and (f) insets were determined by performing linear fit of the data for 0–100 $\mu\text{mol photons m}^{-2} \text{s}^{-1}$ (α) or linear fit to the data at light intensities of 1000–2000 $\mu\text{mol photons m}^{-2} \text{s}^{-1}$. Ek was determined by dividing Pm/ α . Stars represent the statistical significance calculated with respect to WT. * p value < .05; ** p value < .01.

mutants relative to the WT. Specifically, $\Delta srp43$ had the highest yield followed by STR30309 then STR30843 (parallel to F708). Overall, the 77-K results indicate that the loss/modification of cpSRP43 results in a decrease in the antenna pigment-protein complexes (“truncated” antenna phenotype). The elimination of LHCA6 and LHCA7 in STR30843 further decreased the PSI-LHCI signal (relative to the levels in STR30309), which is consistent with more balanced depigmentation between the two photosystems.

The light saturation curve of photosynthesis was measured for STR30309, STR30843, and WT using a Clark-type electrode. Figure 2c,d shows the net oxygen evolution rate of the strains normalized to chlorophyll and AFDW, respectively. Photosynthetic activity in the mutants saturated at a higher light intensity ($E_k \sim 510 \mu\text{mol photons}$

$\text{m}^{-2} \text{s}^{-1}$) compared with the WT ($E_k \sim 300 \mu\text{mol photons m}^{-2} \text{s}^{-1}$). On a Chl basis, STR30843 and STR30309 had >2-fold higher light saturated O_2 -evolution rates ($P_{\text{max}} \sim 720 \mu\text{mol O}_2 \text{ mg Chl}^{-1} \text{ h}^{-1}$) compared with the WT ($358 \pm 16 \mu\text{mol O}_2 \text{ mg Chl}^{-1} \text{ h}^{-1}$) (Figure 2c) parallel to the lower chlorophyll content. Thus, $P_{\text{max}}/\text{AFDW}$ was not significantly different for the three strains (Figure 2d). The mutants did not demonstrate any observable photoinhibition at high measuring light intensities (up to 2000 $\mu\text{mol photons m}^{-2} \text{s}^{-1}$) under the assay conditions used. The initial slope, α (per chlorophyll), is a quantitative measure of light capture and its conversion to O_2 (Weissman & Nielsen, 2016; Macintyre et al., 2002). Mathematically, α is equal to the absorption cross section times the quantum yield. α was marginally higher in the mutants than the WT (Figure 2c inset table).

2.2.3 | Shotgun proteomics

Whole cell shotgun proteomics was used to determine whether the pigment decrease was primarily from lower levels of LHC polypeptides (exclusive decrease in antenna size) or whether reaction centers were also diminished. Biological replicates from two successive days were run for each strain, and the relative label-free quantification (LFQ) intensities were averaged and used for comparison between the strains. Approximately 4000 unique proteins were detected using this extraction procedure. Figure 3a shows the heat map for log₂ fold changes between the various strains normalized to either WT, Δ srp43, or STR30309, as indicated. All cpSRP pathway members including cpSRP54, cpSRP43, cpFTSY, and ALB3.1 had a diminished abundance in the mutant strains demonstrating the importance of cpSRP43 as a central protein for the cpSRP pathway. Interestingly, *P. celeris* has a second cpSRP54-like protein, which remained unchanged. Proteins

related to other systems for transporting proteins across the thylakoid membrane and into the lumen (e.g., SEC and TAT pathway) also remained relatively unchanged (Figure 3a and Table S3).

The peripheral antennae of PSII are in two different aggregation states: trimeric LHCB (identified here as LHCB) and monomeric CP29 and CP26. There exist 5 distinct trimeric LHCB subunit genes in the *P. celeris* genome, two of which show a high degree of homology and are assigned to the same protein in our proteomics data (identified as LHCB_3 here). In WT, LHCB genes are some of the most abundant proteins, with one of the subunits (identified here as LHCB_1) being among the top two highest abundance proteins in *P. celeris*. Upon elimination of cpSRP43, the trimeric subunits showed >4-fold decrease in abundance, whereas the monomeric subunits showed an ~2-fold decrease. This was partially rescued in STR30309 and STR30843, consistent with our Chl a/b ratios. *P. celeris* encodes nine LHCA (PSI associated antenna) proteins, identified here as LHCA1-9. LHCA8 is

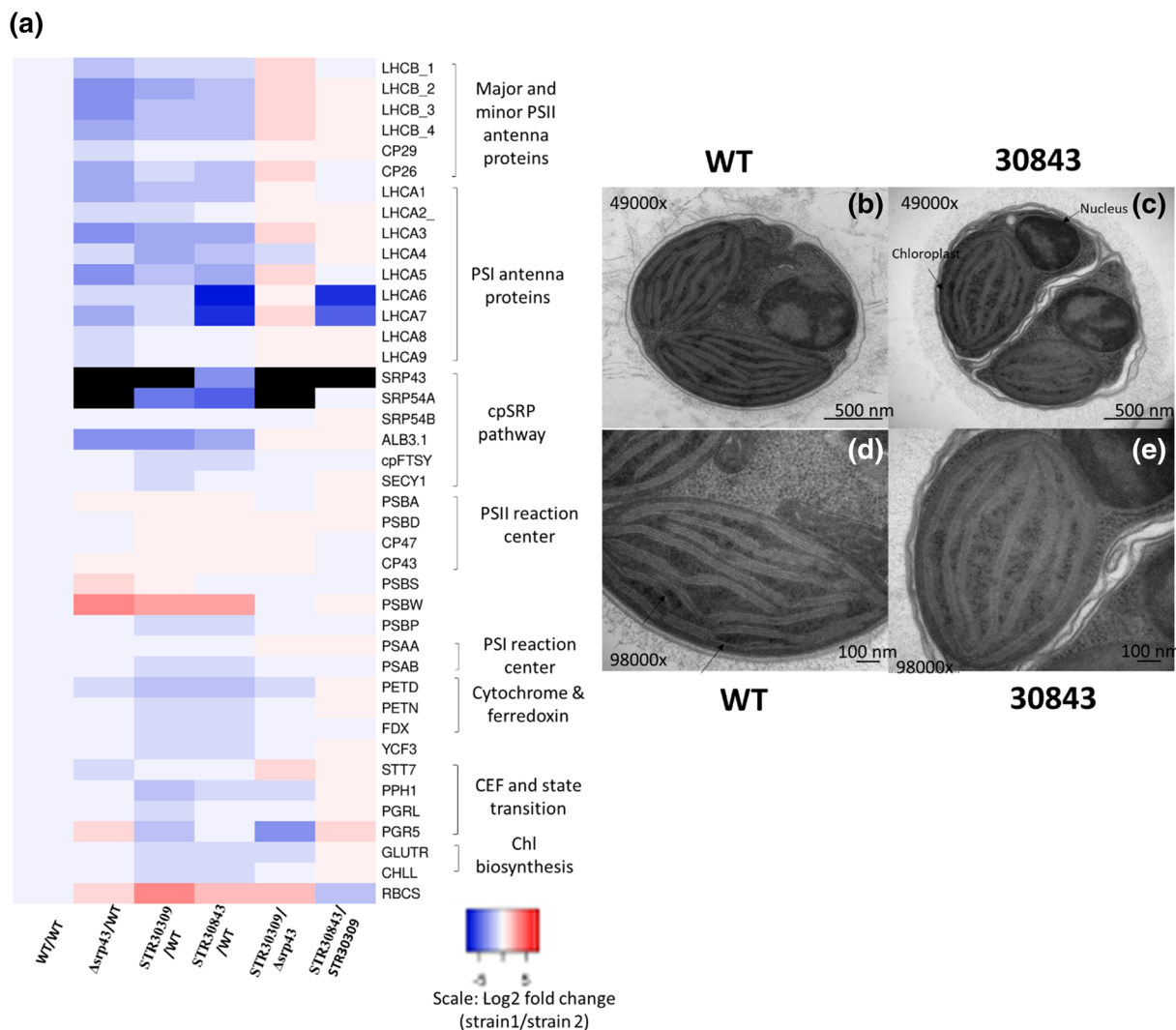


FIGURE 3 (a) Heatmap of differentially expressed proteins between wild type (WT), Δ srp43, STR30309, and STR30843. Log₂ fold change was calculated with respect to either WT (columns 1–4) or Δ srp43 (column 5) or STR30309 (column 6). Protein designations are given on the right side. Proteins undetected in either of the strains are colored black. (b–e) Representative transmission electron microscopic images of the chloroplast ultrastructure in WT and STR30843 sections at magnifications of 49,000 \times or 98,000 \times .

encoded by 3 alleles, whereas all others are encoded by two alleles. Of these, LHCA6 was the most abundant. Similar to LHCs, LHCA proteins (except LHCA9) showed 2- to 8-fold decreases across the three mutants relative to WT. In STR30309, LHCA3, LHCA5, and LHCA7 showed a partial increase as compared with $\Delta srp43$, whereas the remaining subunits remained at a similar abundance relative to $\Delta srp43$. In STR30843, except for LHCA7 and LHCA6 (CAS9 targets), the other LHCs remained at similar levels between STR30309 and STR30843.

Most of the PSII and PSI reaction center proteins remain relatively unchanged across the mutant strains except for the PSAB subunit of PSI, which showed an ~ 1.8 fold decrease. All components of the photosynthetic electron transport chain remained relatively unaffected, except for two subunits of the cytochrome b_6/f complex (petD and petN) and one ferredoxin that demonstrated a slight decrease in abundance. Similarly, most of the Calvin-Benson-Bassham cycle enzymes were unaffected except for one ribulose-bisphosphate carboxylase small chain isoform. Of note was the 2-fold increased abundance of PsbS in $\Delta srp43$ while remaining unchanged in STR30309 and STR30843, suggesting potential activation of NPQ pathways in the former. We were unable to find a gene encoding a homolog of LHCSR, another protein involved in NPQ responses in some algae, in the *P. celeris* genome. Glutamyl t-RNA reductase, a rate-limiting enzyme in chlorophyll biosynthesis and potentially a target of cpSRP43 (Wang et al., 2018), also showed decreased abundance (>2 -fold) in STR30309 and STR30843.

2.2.4 | Transmission electron microscopy (TEM)

To characterize any morphological changes in the thylakoids, STR30843 and WT were imaged using electron microscopy. Samples were harvested from the bioreactors at the 2 p.m. peak of diel illumination (Figure 3b–e). In the WT, thylakoids were organized into 3–4 lamellae that merge and generate larger stacks (up to 8 lamellae). In STR30843, there are long stretches of trilamellar thylakoids with very few to no instances of larger stack formation. Splitting and merging of the thylakoids are infrequently observed suggesting an altered thylakoid architecture in STR30843, consistent with other work where mutants affected in accumulation of antenna proteins are compromised in grana formation (Friedland et al., 2019; Mussgnug et al., 2007; Negi et al., 2020). However, the effect in STR30843 is not as pronounced as in these other organisms.

2.3 | Multiple dilutions throughout the day to improve biomass productivity

To further probe productivity gains in the mutants relative to the WT, multiple, small dilutions were done throughout the diel light period, which lowers overall pigment and biomass concentrations in the bioreactor during illumination. Instead of a single harvest, 10 smaller harvests were performed throughout the day, one at each of the

10 brightest hours. Unlike the single harvest experiments, the changes in pigment and biomass density through the day are less in the multiple harvest mode of cultivation. In addition to maintaining pigment levels throughout the day, this scenario is likely to reflect automated pond operations with frequent harvesting throughout the day (e.g., flocculation or membrane harvesting). With a single harvest, the AFDW at dusk (harvest) is ~ 1 g/L and at dawn is ~ 4 g/L, whereas in the multiple dilution mode, AFDW and pigment concentrations are more constant through the day.

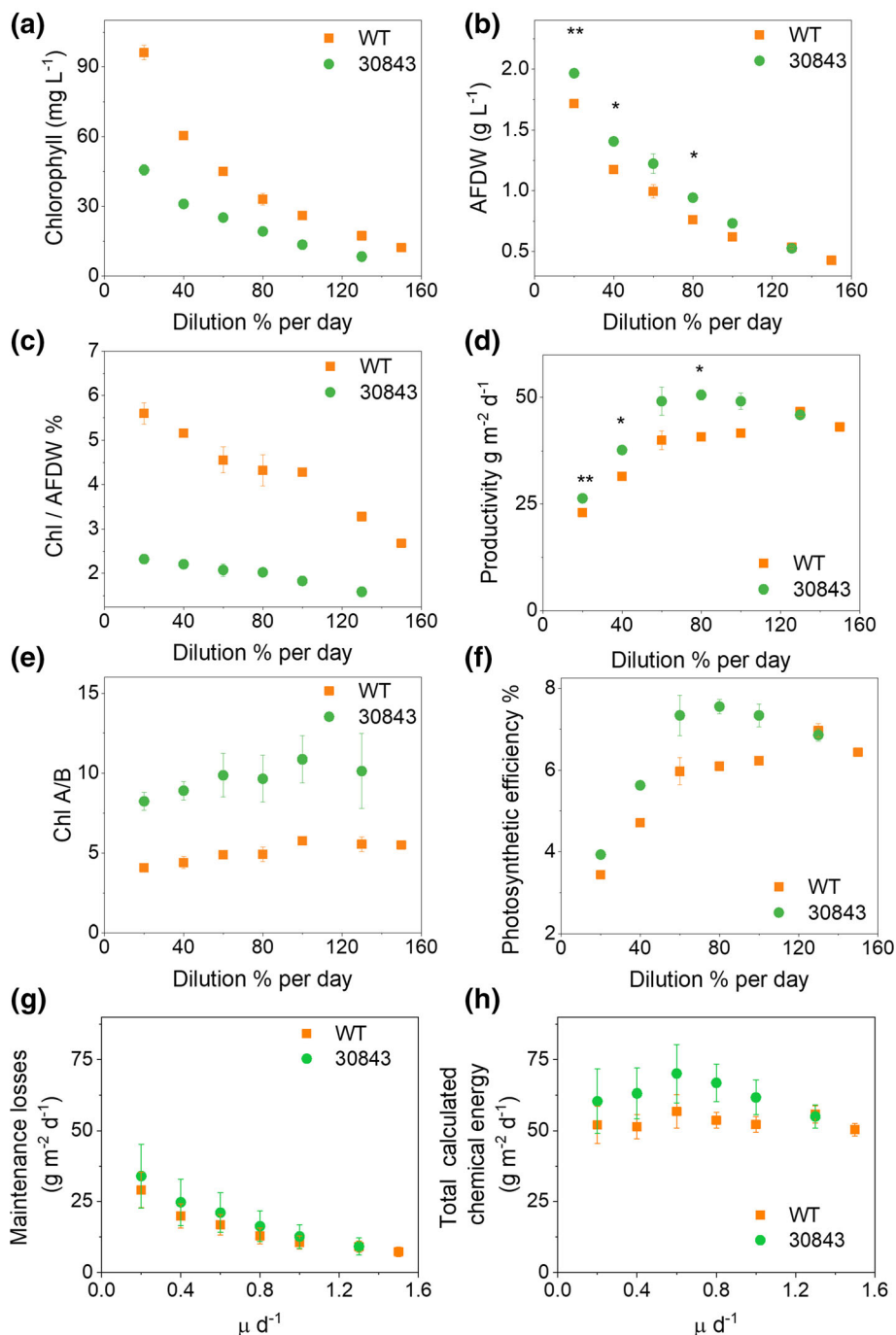
Seven different dilution volumes, 20%, 40%, 60%, 80%, 100%, 130%, and 150%, of the total bioreactor volume (400 ml) were harvested in total across the 10 harvests per day. Cultures were diluted each hour from 9 a.m. to 6 p.m. in the diel script. For example, when performing a 130% dilution, 52 ml of the culture was sampled, and replaced with fresh media, each hour from 9 a.m. to 6 p.m. allowing for the total removal of 520 ml (130%) of culture per day. STR30843 was not run at 150% dilution. Fractions collected throughout the day were composited (pooled together), stored on ice, and used for measuring the average biomass density (AFDW g L^{-1}). Volumetric biomass productivity for each dilution rate was calculated as the product of the average biomass density times the dilution. Aliquots of “2 PM” fractions were harvested and used for measuring *P-I* curves and 77-K fluorescence emission spectra. For all the dilutions, except for WT at 100% and 150%, two separate bioreactor campaigns were undertaken with multiple samplings on consecutive days (3–10 days of sampling for each campaign) for each run after balanced growth was attained (6–20 total biomass samples were measured for each sample). Averages from each bioreactor campaign were used to calculate the final average and standard error, which is equal to the difference between the average value and each data point for $n = 2$.

The influence of the dilution on productivity, AFDW, chlorophyll content, Chl/AFDW, Chl a/b ratio, and PAR-to-biomass conversion efficiency is displayed in Figure 4a–f. As expected, the chlorophyll and biomass densities decreased with increasing dilution (Figure 4b). At all the dilutions tested, STR30843 consistently maintained $>50\%$ lower chlorophyll content than the WT, similar to our observations in the single dilution (60%) experiments. Chl/AFDW decreased with increasing dilution rates for both strains; however, WT was never able to reach the low pigment levels observed for STR30843 (Figure 4c). WT had a Chl/AFDW of $5.6 \pm .2\%$ at 20% total daily dilutions and reached 2.7% Chl/AFDW at 150% total daily dilutions. STR30843 had $2.3 \pm .1\%$ Chl/AFDW at 20% total daily dilutions and reached $1.6 \pm .1\%$ Chl/AFDW at 130% total daily dilutions.

At the dilutions tested, WT displayed a maximum productivity of $46.7 \pm 1.1 \text{ g m}^{-2} \text{ day}^{-1}$ (light to biomass conversion efficiency of $7.0 \pm .2\%$) at the 130% total daily dilutions. Productivity at 130% day^{-1} was significantly different than 20, 40, and 60% day^{-1} dilutions as tested by ANOVA one-way comparison at significance level of .05. Increasing dilution to 150% day^{-1} decreased WT productivity. However, this is probably not due to incomplete absorption of incoming light, which was likely only about 1% (calculated by extrapolating measured optical cross section, which changed little with dilution rate, and the measured chlorophyll content). Thus, the productivity optimum is



FIGURE 4 Growth metrics of STR30843 and wild type (WT) at different dilutions (multiple dilution experiment): (a) chlorophyll content (mg L^{-1}), (b) biomass density ash-free-dry-weight (AFDW) (g L^{-1}), (c) Chl/AFDW%, (d) productivity ($\text{g m}^{-2} \text{ day}^{-1}$), (e) Chl a/Chl b ratio, (f) light-to-biomass conversion efficiency versus daily dilution rate. Each data point represents the average and standard error for two different ALGiSIM runs (biological replicates) with each replicate being sampled on 3–10 consecutive days ($n = 6$ –20 total biomass measurements). Error bars for WT at 100% and 150% are not given due to a single biological replicate with each run having 8–10 daily biomass measurements. Shown for those are the averages calculate from the 8–10 consecutive daily replicates. (g)–(h) represent the (g) calculated maintenance energy and (h) total conversion of light to chemical energy (maintenance energy + measured net productivity) as determined using the Gons and Mur 1965 model. *t*-test *p* value was calculated in (b) and (d) only. Significance was not calculated for 100% and 150% dilutions.



quite broad, with productivity only diminishing at the highest biomass densities (see maintenance discussion below), and at the lowest biomass density, STR30843 also had a broad optimum at about $50 \text{ g m}^{-2} \text{ day}^{-1}$, beginning at $60\% \text{ day}^{-1}$. The $80\% \text{ day}^{-1}$ is statistically not different than 60, 100, and $130\% \text{ day}^{-1}$ dilutions) (Figure 4f). For both strains, productivity at the best tested dilution was around 7–13% higher than the unoptimized 60% single dilution per day (Table 1). At daily dilutions of $100\% \text{ day}^{-1}$ and below, STR30843 had 14–24% higher steady state biomass density as compared with the WT (Figure 4b) and correspondingly higher productivities (statistically significant for all dilutions except $60\% \text{ day}^{-1}$ [for which the two

replicates had higher error than other dilutions]) demonstrating that this depigmented strain performed better under dense culture cultivation conditions.

The decrease in biomass yields, commonly found at low dilutions (or high biomass densities), may occur because of an increasing fraction of the converted chemical energy getting directed towards maintenance, that is, functions other than growth (Gons & Mur, 1975; Pirt, 1986). To determine the fraction of energy consumed for cell maintenance, we fit our data (Figure 4a–f) to the model described in Gons and Mur (1975), where the total absorbed light is assumed to be used for growth (observed biomass productivity = specific growth

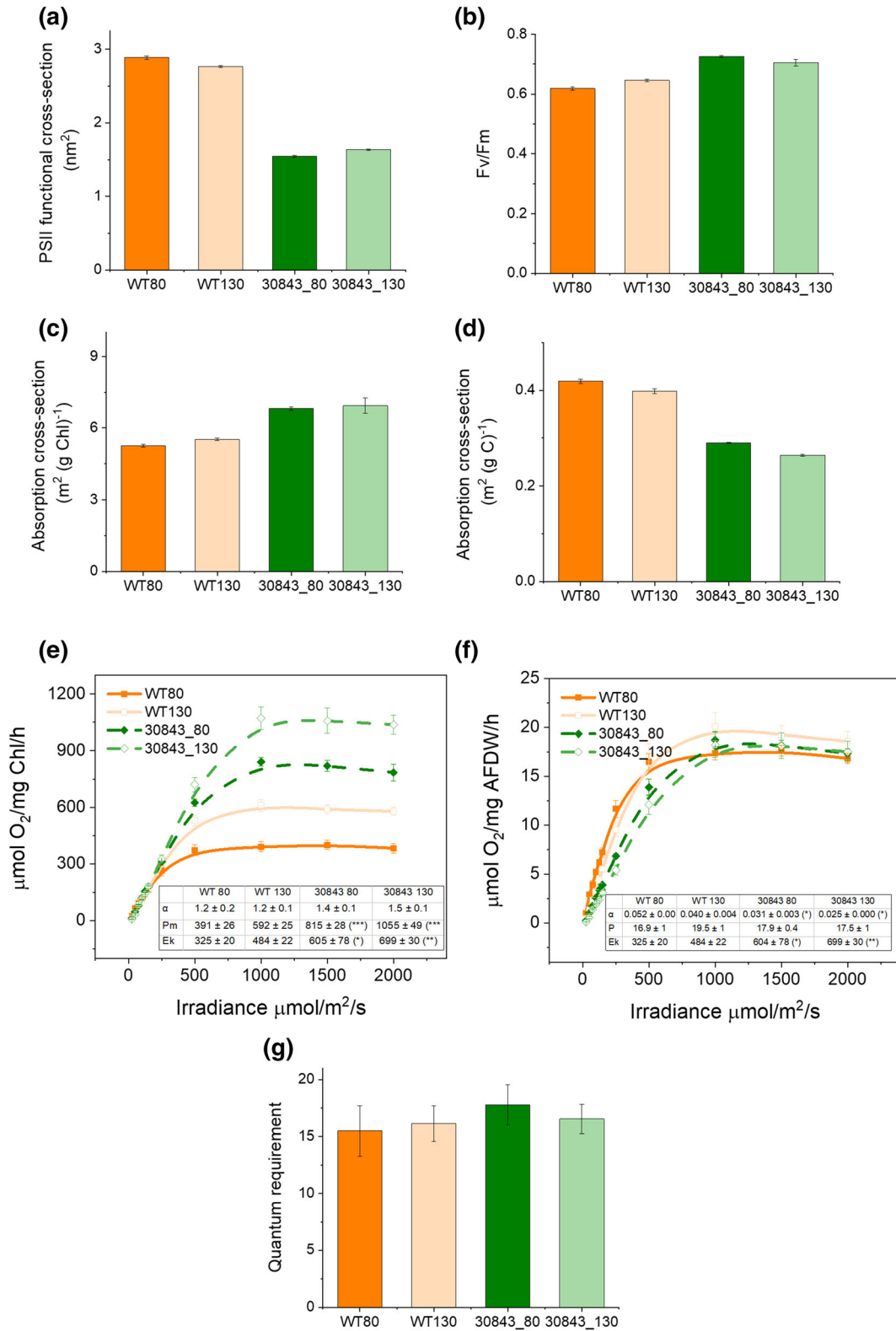


FIGURE 5 Legend on next page.



rate \times steady-state biomass density) or for cell maintenance (specific maintenance coefficient \times steady-state biomass density). When the total light energy absorbed per unit energy stored in biomass is plotted as a function of specific growth rate, the slope of the line determines the efficiency of light conversion, and the y -intercept times slope represents maintenance coefficient (Data S1 Methods). The specific maintenance coefficient times the areal biomass density gives the maintenance energy, and specific growth rate times the areal biomass density determines the areal productivity. The total of maintenance energy and biomass productivity gives the total light energy converted to chemical energy (see Data S1 Methods for calculations). Figure 4g,d,h are the calculated maintenance energy, biomass productivity, and the total conversion of photosynthetic energy to chemical energy. Maintenance coefficients ($.25 \pm .05 \text{ day}^{-1}$ for WT and $.26 \pm .09 \text{ day}^{-1}$ for STR30843) and slopes ($12.6 \pm .8$ for WT and 10.4 ± 2.7 for STR30843, p value = .12) were statistically not different for the strains (calculations given in Data S1 Methods) indicating that the STR30843 transformations did not affect maintenance significantly. As expected at lower dilutions, the energy used for maintenance (Figure 4g) is high, even higher than the net productivity (Figure 4d) while decreasing at higher dilutions. Of note is that up to dilutions of $100\% \text{ day}^{-1}$, the total chemical energy generated by WT remained relatively unchanged at $\sim 52\text{--}55 \text{ g m}^{-2} \text{ day}^{-1}$ indicating that the changes in the photosynthetic efficiency observed (Figure 4f) were an outcome of changes in maintenance requirements rather than changes in light transmittance.

To understand the effect of the altered dilution regimes on the photosynthetic apparatus of STR30843 and WT, functional absorption cross section and optical absorption cross sections for the composited samples were determined using fluorescence induction kinetics and an integrating sphere, respectively; 77-K fluorescence analysis and $P-I$ curves were performed on samples harvested at 2 p.m. in the solar simulated day. Photosystem II functional cross sections estimated using fluorescence induction fast repetition rate fluorometer (FRRF) were 2-fold smaller in STR30843 as compared with WT across the dilutions (Figure 5a). F_v/F_m , a measure of the maximum quantum efficiency of PSII, was slightly higher for the mutant as compared to the WT (Figure 5b). The optical absorption cross section as determined using an integrating sphere demonstrated that STR30843 indeed had a lower absorption cross section per carbon however, higher absorption cross section per Chl [$\text{m}^2 (\text{gChl})^{-1}$] as compared with the WT (Figure 5c,d). This difference suggests the involvement of pigment packaging effects in the WT strain; 77-K data as well as $P-I$ curves show that upon higher

dilution, both WT and STR30843 transition to a higher light acclimation state with lower Chl/AFDW (Figure 5), higher P_{max} (per Chl), a decrease in initial slope in the O_2 -evolution/AFDW curve, and a lower PSI-LHCI (Figure S4A, F708 nm peak). However, optical cross sections for each strain did not change much with dilution rate (from 80 to $130\% \text{ day}^{-1}$), despite a 25% decrease in chlorophyll/AFDW at the higher dilution rate for each strain. This may be due to the relative increase in carotenoids at the higher rate of dilution (see below). $P_{\text{max}}/\text{AFDW}$ remained unchanged across the dilutions indicating that irrespective of the light history of the culture (Figure 5f), the mutant and the WT retain high photosynthetic rates that seem to easily sustain high specific growth rates. Additionally, at the highest productivities (continuous dilution conditions of $130\% \text{ day}^{-1}$ for WT and $80\% \text{ day}^{-1}$ of STR30843), STR30843 consistently had less LHCII and PSI-LHCI as compared with the WT. The quantum requirement (photons per O_2) under dense culture conditions was estimated from the initial slope of the $P-I$ curves and the absorption cross section (Figure 5e inset table). Both the WT and STR30843 had similar minimum quantum requirements (maximum quantum efficiency) suggesting no significant difference in the balance between the two photosystems. E_k values for the WT at 80 and $130\% \text{ day}^{-1}$ dilution were significantly different at 326 ± 20 and 484 ± 22 , respectively (p value .006). However, the E_k values for STR30843 at 80% (605 ± 78) and 130% (699 ± 30) were not (p value .3).

Carotenoid content was also quantified under 80 and $130\% \text{ day}^{-1}$ dilutions on the composited samples (Figure S4B). On an AFDW basis, carotenoids were $1.1 \pm .1\%$, $1.1 \pm .1\%$, $.8 \pm .1\%$, and $.9 \pm .1\%$ of AFDW for WT at dilution rates of $80\% \text{ day}^{-1}$, WT at $130\% \text{ day}^{-1}$, 30843 at $80\% \text{ day}^{-1}$, and 30843 at $130\% \text{ day}^{-1}$, respectively. Except for a decrease in antheraxanthin content at higher dilutions, the overall pigment composition remained relatively similar between the dilutions for both the strains. Carotenoid/chlorophyll ratios were $.25 \pm .02$, $.32 \pm .03$, $.38 \pm .01$, and $.55 \pm .05$ for WT $80\% \text{ day}^{-1}$, WT at $130\% \text{ day}^{-1}$, 30843 at $80\% \text{ day}^{-1}$, and 30843 at $130\% \text{ day}^{-1}$ dilutions, respectively, indicating that at higher dilutions, the carotenoid fraction increases relative to chlorophyll. Additionally, 30843 had a higher ratio of carotenoids to chlorophylls.

3 | DISCUSSION

Light saturation of photosynthesis, which is exacerbated in lower-light acclimated states, is a major problem that limits algal productivity in mass cultures (Grobelaar, 2010; Grobelaar et al., 1995; Kirst

FIGURE 5 Characterization of wild type (WT) and STR30843 at 80% or 130% continuous dilution. (a) PSII functional absorption cross section. (b) F_v/F_m . (c) Absorption cross section, normalized to total chlorophyll. (d) Absorption cross section, normalized to particulate organic carbon. (e, f) Photosynthesis-Irradiance curves, normalized to total chlorophyll and ash-free-dry-weight (AFDW), respectively. (g) Maximum quantum requirement, determined from α and absorption cross section. Each data point represents the average and standard error for two separate bioreactor runs with 3–4 daily replicates sampled (6–8 total measurements). Data represent average and standard error of the net oxygen evolution rate for 3 daily replicates. Chlorophyll density of the suspension for the $P-I$ experiment was $\sim .6\text{--}.7 \mu\text{g ml}^{-1}$. Parameters given in (e) and (f) insets were determined by performing linear fit of the data for $0\text{--}100 \mu\text{mol photons m}^{-2} \text{ s}^{-1}$ (α) or linear fit to the data at light intensities of $1000\text{--}2000 \mu\text{mol photons m}^{-2} \text{ s}^{-1}$. E_k was determined by dividing P_m/α . Stars represent the statistical significance calculated with respect to WT. * p value $< .05$, ** p value $< .01$, *** p value $< .001$.

et al., 2017; Melis, 2009; Weissman, 1978; Weissman & Nielsen, 2016). This has prompted research into developing strains with permanently truncated peripheral antenna (and decrease in the number of reaction centers if necessary) to minimize pigment content so as to increase the irradiance at which photosynthesis saturates. *P. celeris* is currently among the most promising outdoor biomass production strains due to its high productivity and robustness in cultivation (46), and we have initiated a series of pigment lowering efforts to further improve biomass productivities. By targeting the molecular chaperone cpSRP43 using CAS9, we were able to simultaneously attenuate protein levels of both PSII and PSI peripheral antenna subunits generating mutants with >50% loss in pigmentation and no significant changes in the remaining photosynthetic machinery under our assay conditions (Table 1, Figures 1, 3, and 4). cpSRP43 knock-outs have been previously used to generate truncated antenna mutants in other photosynthetic organisms including *Arabidopsis thaliana*, *Nicotiana tabacum*, and *Chlamydomonas reinhardtii* (Amin et al., 1999; Kirst, Garcia-Cerdan, Zurbriggen, Ruehle & Melis, 2012; Kirst et al., 2018; Klimyuk et al., 1999). Interestingly, our CAS9 strategy yielded two phenotypically distinct depigmented mutants resulting from the variations in editing: (i) a complete homozygous knock-out of cpSRP43 (Δ srp43) and (ii) a modified version of cpSRP43 that had a single amino acid inserted at the cut site (STR30309) in one allele; whereas the second allele was undetected by PCR (Figure 1). While Δ srp43 had a severe >75% lower pigment levels, the modified version of cpSRP43 (STR30309) demonstrated a smaller decrease in total pigments (~65% decrease) and had a lower Chl a/b ratio (Figure 3). Differences in Chl a/b ratios and the abundances of LHC proteins between Δ srp43 and STR30309 indicate the ability of the modified SRP43 protein to partially rescue protein function (Figures 1 and 3, Table 1).

Even with the complete loss of the cpSRP43, Δ srp43 accumulated all the LHC proteins, albeit at lower concentrations, suggesting the presence of an additional SRP43-independent pathway for LHC transport in *P. celeris*. Existence of a such pathway has been alluded to in *Chlamydomonas* though a mechanism that remains elusive (Bujaldon et al., 2020; Kirst & Melis, 2014). Strains with one WT copy of the protein and the other allele eliminated exhibited normal pigmentation, indicating that the single cpSRP43 amino acid insertion in STR30843 (Figure S2) is the causative agent of the intermediate phenotype. Variations in chaperoning ability of cpSRP43 caused by point mutations have been demonstrated in vitro (McAvoy et al., 2018). Shin et al. (2016) found a point mutation in cpSRP43 protein of a depigmented *Chlorella* strain (~50% lower pigments) despite this strain having high levels of cpSRP43 expression. Identification and use of modulated function mutants that generate phenotypes intermediate of a complete knockout and WT may be a useful strategy to fine tune pigment levels in photosynthetic organisms and identify improved biomass strains.

Both STR30309 and STR30843 had higher chlorophyll normalized α (initial slope of the P-I curve), higher E_k , and no significant effect on the P_{max} per AFDW (Figure 2) suggesting that at least the photosynthetic efficiency as well as the coupling of the photosystems to CO₂ fixation is not significantly affected in these strains. This is

consistent with the proteomics data that show only minor changes in the levels of proteins in the photosynthetic electron transport chain and Calvin Benson Bassham cycle. Genotypically, the difference between STR30309 and STR30843 was the further elimination of LHCA7 and LHCA6 from the STR30309 strain by CAS9. No significant differences in the reaction center proteins were observed for the two strains (Figure 3a), and the 77-K fluorescence profile suggested changes in the relative PSI-LHCI levels in STR30843 (Figure 2b). This indicates that the increase in productivity (PAR-to-biomass conversion efficiency) observed in STR30843 as compared with STR30309 (Table 1) is most likely a direct outcome of better balance between LHCI-PSI and LHCI-PSII light absorption. These results reinforce the idea that depigmentation is necessary, but not a sufficient condition for higher productivity, and needs to be complemented with the balanced absorption of light between the two photosystems. Currently, we are continuing to target additional LHCAs in Δ srp43 and STR30843 to determine if photosystem excitations can be balanced further.

It was recognized in early work (Cook, 1951; Dabes et al., 1970; Eppley & Dyer, 1965; Myers & Graham, 1959; Weissman & Benemann, 1979) that when biomass productivity is measured as a function of specific growth rate (which is equal to dilution rate in continuously operated algal cultures), there is usually an optimum. This optimum may be narrow (Cook, 1951; Eppley & Dyer, 1965). Presumably at low dilution rates (high biomass densities), productivity declines due to high maintenance burden. At higher dilution rates, productivity may also decrease due to photoinhibition and eventually because as dilution rate approaches the maximum specific growth rate of the organism under the growth conditions, not all of the incident light is absorbed by the culture. Myers and Graham (1959) recognized that the cells may also acclimate to the different average light levels in the reactor at different dilution rates, broadening out the productivity optimum. They pointed out that algal cells acclimated to higher light, having lower pigment/AFDW ratios, have a higher saturating irradiance and hence higher photosynthetic efficiency leading to this broader optimum. None of these earlier studies imposed a diel light regime, but the underlying principles remain similar.

The data in Figure 4c show that both the WT and STR30843 have decreasing chlorophyll/AFDW ratios with increasing dilution rate; that is, the chlorophyll content of the cells is acclimating to the different light levels. However, these changes in chlorophyll content are mitigated by pigment packaging effects. Lower chlorophyll/AFDW increases the optical cross section per unit chlorophyll, which diminishes the decreases in this cross section based on biomass density. Increases in the ratio of other pigments to chlorophyll also increase the optical cross sections. The ratio of lutein and β -carotene to chlorophyll increases in both the WT and 30843 with dilution rate (Figure S4C). The consequence is that the light acclimation observed may broaden the optimum of biomass productivity versus specific growth rate but may not increase the actual productivity of these higher light acclimation states by very much, if at all. All these factors led to a very flat response of biomass productivity with dilution rate, over a large range of the latter, for both strains studied here. Within



these broad optima, increases in biomass density were nearly proportional to decreases in specific growth rate. In fact, there was very little change in biomass productivity for dilution rates above 40% day⁻¹ with either the WT or 30843, like an earlier study with a *Chaetoceros* species under diel conditions (Weissman & Nielsen, 2016). There may have been such a decrease for STR30843 at high light (high μ), in terms of total chemical energy (maintenance plus net productivity, Figure 4h).

Depigmented cells with a “truncated antenna” phenotype absorb fewer photons per cell, leading to less loss due to light saturation. Inter strain comparisons of the productivity of a WT with a depigmented strain can be done in several ways. One way is to compare them for cases for which the light profile in the reactor runs is similar; that is, the extinction coefficient for light attenuation (the absorption cross section times the biomass density) is the same. The specific growth rate in mass culture, or any column containing algae, is governed by the light profile within the reactor and the physiological responses to this light profile of the alga under study including its maintenance burden, sensitivity to high irradiance, and factors that affect the minimum quantum requirement. Of interest here is to try to isolate the potential increases in biomass productivity of the depigmented strain due to lowered light saturation losses, from the other factors affecting productivity (maintenance burdens and photoinhibition). A comparison of the productivity at moderate specific growth rates (dilution rates) does this.

The WT and STR30843 are compared at a dilution rate of 80% day⁻¹ in Case 1 of Table 2. The light profiles, that is, extinction coefficients, were similar. Strain 30843 produced 24% more biomass and had a total chemical energy (maintenance plus biomass) also 24% higher. When the strains were compared at 60% day⁻¹ dilution rates, the results were similar (23% higher for STR30843, data not shown in the table). This increase may be taken to represent the impact of

differential light saturation on increasing productivity with about 55% lower chlorophyll content.

The two strains are compared on a different basis: equal but relatively high AFDW densities in Case 2. The WT can attain an average specific growth rate of 40% day⁻¹, whereas the de-pigmented 30843 attains 60% day⁻¹. Thus, the biomass productivity of the latter is about 50% higher, and the total chemical energy is 36% higher. In this situation, the maintenance burdens are about the same because they are based on biomass density. The larger increase in productivity than in Case 1 may be attributed to not only the depigmentation of 30843 but also to the even lower state of light acclimation of the WT in this case than in Case 1. The former leads to less loss due to light saturation of the depigmented strain and the latter to increased losses of the WT.

In Case 3, the comparison is again based on equal AFDW densities but much lower ones. Again, the maintenance burdens are the same for the strains, but there is almost no increase in biomass productivity nor total chemical energy conversion from strain 30843 despite the lower pigmentation (by a factor of two) and lower cross section/AFDW (by almost one-third). The extinction coefficient for 30843 is much lower, which is expected due to the substantially lower chlorophyll density. But the average specific growth rates attained are the same despite the large difference in average irradiance in the reactor (extinction coefficient). The mismatch between extinction coefficients and average specific growth rates reflects a very different physiological response to the light field. Here, it may be that strain 30843 is experiencing more photoinhibition than the WT.

Except for a couple of studies (Cazzaniga et al., 2014; Huesemann et al., 2009; Negi et al., 2020), most of the research reported for depigmented strains uses constant light levels. Our bioreactor results clearly show that the depigmented strains display higher productivity than WT under dense culture-diel light conditions (Table 1, Figure 4)

TABLE 2 Selected comparisons of WT versus STR30843 reactor trials.

	Case 1		Case 2		Case 3	
	WT 80	30843 80	WT 40	30843 60	WT 130	30843 130
Chl density, mg L ⁻¹	33.1	19.2	60.4	25.2	17.3	8.4
^a K, m ⁻¹	150	131	~300	~170	96	58
Chl, %AFDW	4.3	2.0	5.2	2.1	3.3	1.6
AFDW, g L ⁻¹	.76	.94	1.18	1.22	.54	.53
m ² (gChl) ⁻¹	5.25	6.8	~5.0	~6.7	5.53	6.94
m ² (gAFDW) ⁻¹	.196	.136	~.24	~.15	.177	.116
Biomass productivity, g m ⁻² day ⁻¹	40.8	50.7	31.5	49.1	46.7	45.9
m, g m ⁻² day ⁻¹	12.9	16.3	19.9	21.0	9.1	9.1
Total energy, g m ⁻² day ⁻¹	53.7	66.8	51.4	70.1	55.7	55.0
Ratio, productivity ^b	1.24		1.56		.98	
Ratio, total energy ^b	1.24		1.36		.98	

Abbreviations: AFDW, ash-free-dry-weight; WT, wild type.

^aK calculated by multiplying chlorophyll density times optical cross section.

^bFor each case, the ratio was calculated by dividing the 30843 values by WT value.

and underscore the need for optimizing dilution regimes for each type of strain for maximizing productivity.

In summary, through systematic engineering, we were able to generate a highly depigmented strain of *P. celeris* that under dense diel light conditions, outperformed the already high wild type (WT) with biomass productivity gains of 5–24% and achieving bioreactor yields of $50 \text{ g m}^{-2} \text{ day}^{-1}$. The highest productivities for STR30843 were achieved at moderate dilution rates, that is, denser cultures. At dilutions of $100\% \text{ day}^{-1}$ or lower, STR30843 consistently maintained higher biomass density (14–24%) and productivity (14–24%) and demonstrated better light utilization as compared to the WT at equivalent dilution rates (Table 1, Figure 4). E_k values remained consistently higher than the WT. The advantages of depigmentation might be partially negated by other factors such as enhanced carotenoid fraction relative to chlorophyll (Figures 4 and 5) or enhanced photoinhibition and needs to be probed further. While STR30843 did not have the dramatic alterations in thylakoid membrane architecture upon the loss/decrease of LHCs as observed in prior work (Asakura et al., 2004; Friedland et al., 2019; Mitra et al., 2012; Mussnug et al., 2005, 2007; Negi et al., 2020), the thylakoid branching was affected, and additional research is required to probe how changes in the architecture of the thylakoids may affect cell physiology, connectivity of photosystems, and electron conduction (Figure 3b–e). The genetic alterations did not change the maintenance burden of the STR30843 compared with the WT, and the maintenance burden was low for both. This minimizes any penalty for operating the modified strain at higher biomass density than the WT. Thus, from a practical standpoint, productivity gains by the altered strain are attainable, whereas achieving the maximum productivity of the WT requires more dilution than is practical. The >50% decrease in pigments coupled with higher productivity without significant effect on respiration relative to WT under dense cultivation makes STR30843 a useful chassis strain to further pursue higher productivities in depigmented strains with balanced photosystem activities.

4 | MATERIALS AND METHODS

4.1 | Algal batch culture conditions

All strains were routinely maintained in shake flasks kept in 1% CO_2 /air atmosphere and exposed to $600\text{--}800 \mu\text{mol m}^{-2} \text{ s}^{-1}$ (PAR) 33°C . Dense culture medium composed of 40 g L^{-1} Instant Ocean® sea salt, 15 mg L^{-1} $\text{FeSO}_4 \cdot 7\text{H}_2\text{O}$ (stock solution of 2 g L^{-1} made in 2.7 g L^{-1} EDTA), $313.8 \mu\text{g L}^{-1}$ $\text{MnSO}_4 \cdot \text{H}_2\text{O}$, $24.23 \mu\text{g L}^{-1}$ $\text{CoCl}_2 \cdot 6\text{H}_2\text{O}$, $48.82 \mu\text{g L}^{-1}$ $\text{ZnSO}_4 \cdot 7\text{H}_2\text{O}$, $2 \mu\text{g L}^{-1}$ $\text{CuSO}_4 \cdot 5\text{H}_2\text{O}$, $6.81 \mu\text{g L}^{-1}$ $\text{Na}_2\text{MoO}_4 \cdot 2\text{H}_2\text{O}$, 89 mg L^{-1} KH_2PO_4 , 436 mg L^{-1} urea, 4.4 mg L^{-1} vitamin B12, $4.4 \mu\text{g L}^{-1}$ biotin, $1.54 \mu\text{g L}^{-1}$ thiamine (vitamin B1), and 100 mg L^{-1} kanamycin was used for liquid culturing. For maintenance on solid media, the strains were cultured on QATM plates (Krishnan et al., 2021).

4.2 | Transformant generation and screening

Phased diploid genome sequence for *P. celeris* has been published previously (accession number PRJNA598876) (Becker et al., 2020). Target-specific knockout transformants were generated and screened using the protocol described in (Krishnan et al., 2020), (Ajjawi et al., 2017). For RNP based editing, 50 pmols of preassembled RNP complexes along with $3 \mu\text{g}$ of linearized selectable-marker plasmid (nourseothricin selection marker described in Krishnan et al., 2020) and 5×10^8 sorbitol washed cells were electroporated in a 2 mm cuvette at 1300 V and time constant of 25 ms. After 6 h of recovery in QATM medium, transformants were plated with top agar overlay containing 75 mg L^{-1} nourseothricin and grown at $\sim 50 \mu\text{mol m}^{-2} \text{ s}^{-1}$ PAR in a $30^\circ\text{C}/1\% \text{ CO}_2$ chamber for 3 weeks. Single colonies were picked and restreaked onto selective plates, then screened by colony PCR for target gene insertions/deletions (indels).

4.2.1 | Generation of the *Picochlorum* CAS9 editor strain STR30208, STR30309, and STR30843

The *Picochlorum* Cas9 editor line (STR30208) was generated by random integration of an *Ascl* restriction enzyme linearized vector, pSlicePico, harboring expression cassettes for the selectable marker blasticidin deaminase (BSD) and Cas9 (Ajjawi et al., 2017). The expression of BSD and CAS9 genes was driven by the endogenous promoters and terminators for Rubisco Small Subunit 1 and LHCII, respectively. Transformation of the linearized construct by electroporation was conducted as described previously (Ajjawi et al., 2017). Colonies were selected on solid agar media containing 500 mg L^{-1} blasticidin. STR30208 was chosen as the best expressor and carried forward as the editor line.

To generate SRP43 mutants, STR30208 was transformed with guide RNA targeting the *SRP43* gene (Table S1) and a PCR product encoding the selectable zeocin resistance (ZeoR) marker gene optimized for *P. celeris* codon usage. The expression of the ZeoR gene was driven by the endogenous promoter and terminator for Rubisco Small Subunit 1. Colonies were selected on solid agar media containing 50 mg L^{-1} zeocin and screened by PCR sequencing for indels and knock-in disruptions. STR30309 was identified as a phenotypically unique mutant. STR30309 was found to have a single amino acid insertion in one allele.

To generate LHC knockout combinations stacked with the SRP43 phenotype, the mutant strain STR30309 was transformed with guide RNAs targeting six different LHC genes (Table S1) and a PCR product encoding the selectable nourseothricin resistance gene (Nat1) sequence optimized for algae. The expression of the Nat1 gene was driven by the endogenous promoter and terminator for LHCII. Colonies were selected on solid agar media containing 75 mg L^{-1} nourseothricin and screened by PCR sequencing for indels and knock-in disruptions. STR30843 was found to be a homozygous mutant for two LHCs, *LHCA6* and *LHCA7* (pending patent application [Kuzminov



et al., 2022)]. Gene sequences for cpSRP43, LHCA6, and LHCA7 from *P. celeris* are given in Data S2.

Primers and plasmids used in the study are given in Tables S1 and S2. Data S3 gives the complete DNA sequences for the plasmids used in this study.

4.3 | ALGiSIM (photobioreactor) runs

A custom built, solar-simulating, bench scale photobioreactor (ALGiSIM) was used to analyze the physiological characteristics of the strains in diel conditions as described previously (Cano et al., 2021). For all experiments, algae were grown in 400-ml square Pyrex bottles with a light pathlength of 6.7 cm, maintained at 33°C and continuously sparged with 2.25% CO₂ enriched air at 350 ml/min. Contents of the reactor were well mixed using a magnetic stir bar. The pH was maintained between 6.8 and 7.2. Cool white LED panels on the side provided PAR and diel illumination. ALGiSIM is equipped with computer controlled liquid handling systems capable of performing automatic sampling and culture dilutions.

For single dilution experiments, cultures were diluted every day by removing 60% of the culture volume (after replenishing evaporative losses with deionized water) and replacing it with fresh medium. Dilution and harvesting were performed 1 h before sunset. For multi-dilution cultivation, samples were diluted every hour during the 10 brightest hours of the day (from 9 a.m. to 6 p.m.). Cumulatively, the dilutions combined account for a fixed % dilution per day. For example, for a 100% dilution, 40 ml of the culture was removed every hour (from 9 a.m. to 6 p.m., 400 ml total) and replaced with fresh media. Harvested cultures were analyzed for AFDW, pigment content, and photophysiology (Krishnan et al., 2021). The volumetric biomass productivity for the multiple dilution experiment was calculated by multiplying the total biomass removed (collected) by the dilution factor and then multiplying by 67 L m⁻² to get the areal biomass productivity. AFDW, chlorophyll, and carotenoid content were determined as described in Cano et al. (2021).

PAR-to-biomass conversion efficiency is defined as the energy stored in biomass divided by the total energy supplied in the form of light. PAR insolation (mol photons m⁻² day⁻¹) was calculated by integrating the light curve (Figure 1g) over the entire day. This was multiplied by 217 kJ mol⁻¹ photons (PAR) to get the effective supplied energy. An average density of 23 kJ g⁻¹ was used to calculate the energy stored as algal biomass each day.

Maintenance energy calculations were done according to Pirt (1986). See Data S1 Methods for detailed calculations.

4.4 | Photosynthesis-irradiance curve

Photosynthetic oxygen evolution rates were measured using a Clark-type electrode (Weissman et al., 2018). For sample preparation, 1.5-ml culture aliquots were purged with 1% CO₂/helium for 30 s followed by the addition of 12 µl of .5-M sodium bicarbonate as

described in (Weissman et al., 2018). The sample was sparged again for another 20 s and then injected into the sample cell using a gas tight syringe. Following an initial dark period, stepped light intensities (25, 50, 75, 100, 125, 150, 250, 500, 1000, 1500 and 2000 µmol photons m⁻² s⁻¹) were applied for 3 min followed by 3 min of dark. The temperature was maintained at 33°C throughout the experiment. α was determined by performing linear fit of the data for 0–100 µmol photons m⁻² s⁻¹ and P_{max} by averaging values between 1000–2000 µmol photons m⁻² s⁻¹. E_k was determined by dividing P_{max}/ α . Optical absorption and PSII functional cross section were measured as described in Weissman et al. (2018). Quantum yield was calculated by dividing α by optical absorption cross section. Quantum requirement is the inverse of quantum yield.

4.5 | 77-K fluorescence

Cultures were adjusted to 5 µg ml⁻¹ chlorophyll, incubated in dark for 10 min, and flash-frozen in liquid nitrogen. Steady-state fluorescence emission spectra were recorded using Fluorolog at an excitation wavelength of 440 nm.

4.6 | TEM

TEM was performed at the microscopy core facility at CU Boulder. Samples were harvested from the ALGiSIM at 2:15 p.m. of the scheduled day when the cells were exposed to the maximum light intensities. At the time of harvest, the light intensity was ~2400 µmol photons m⁻² s⁻¹; 50-ml samples were placed on an ice bath (in dark) and transported to the EM facility. Samples were high pressure frozen using a Wohlwend Compact O₂ high pressure freezer (Technotrade International, Manchester, NH) as described previously (Giddings et al., 2017). Frozen specimens were then freeze-substituted in anhydrous acetone containing 2% osmium tetroxide and .2% uranyl acetate and embedded in Epon/Araldite resin. Serial thin (80 nm) sections were cut using a Leica UCT ultramicrotome. The serial sections were collected on Formvar-coated copper slot grids, poststained with 2% aqueous uranyl acetate followed by Reynold's lead citrate and imaged using a Tecnai T12 Spirit TEM, operating at 100 kV.

4.7 | Proteomics analysis

Proteomics analysis was performed at the University of Colorado, Boulder proteomics facility. Briefly, .5-ml cell pellets were solubilized, reduced and alkylated using 5% (w/v) sodium dodecyl sulfate (SDS), 10-mM tris(2-carboxyethylphosphine) (TCEP), 40-mM 2-chloroacetamide, 50-mM Tris-HCl, pH 8.5 with boiling 10 min, then incubated shaking at 1000 rpm at 37°C for 30 min. Extracted proteins were digested using the SP3 method (Hughes et al., 2014). Briefly, 200-µg carboxylate-functionalized SpeedBeads (Cytiva Life Sciences) were added followed by the addition of acetonitrile to 80%

(v/v) inducing binding to the beads. The beads were washed twice with 80% (v/v) ethanol and twice with 100% acetonitrile. Approximately 50 µg of protein was digested in 50-mM Tris-HCl, pH 8.5, with .5-µg Lys-C/Trypsin (Promega) and incubated at 37°C overnight. Tryptic peptides were desalted with the addition of 95% (v/v) acetonitrile binding the peptides back to the beads and washed once with 100% acetonitrile. Peptides were collected from the beads with two elutions of 1% (v/v) trifluoroacetic acid, 3% (v/v) acetonitrile. Cleaned peptides were then dried in a SpeedVac vacuum centrifuge and stored at -20°C until analysis.

4.8 | Mass spectrometry analysis

Tryptic peptides were suspended in 3% (v/v) ACN and .1% (v/v) trifluoroacetic acid (TFA) and directly injected onto a reversed-phase C18 1.7 µm, 130 Å, 75 × 250 mm M-class column (Waters), using an Ultimate 3000 nanoUPLC (Thermo Scientific). Peptides were eluted at 300 nl/min with a gradient from 2% to 20% ACN in 100 min then to 32% ACN in 20 min then 1 min to 95% ACN and detected using a Q-Exactive HF-X mass spectrometer (Thermo Scientific). Precursor mass spectra (MS1) were acquired at a resolution of 120,000 from 380 to 1580 *m/z* with an automatic gain control (AGC) target of 3E6 and a maximum injection time of 45 ms. Precursor peptide ion isolation width for MS2 fragment scans was 1.4 *m/z*, and the top 12 most intense ions were sequenced. All MS2 spectra were acquired at a resolution of 15,000 with higher energy collision dissociation (HCD) at 27% normalized collision energy. An AGC target of 1E5 and 100-ms maximum injection time was used. Dynamic exclusion was set for 25 s with a mass tolerance of ±10 ppm. Raw files were searched against the custom *P. celeri* database using MaxQuant v.2.0.3.0. Cysteine carbamidomethylation was considered a fixed modification, and methionine oxidation and protein N-terminal acetylation were searched as variable modifications. All peptide and protein identifications were thresholded at a 1% false discovery rate (FDR).

4.9 | Data analysis

Standard error of mean has been used all through. Statistical inferences are calculated using *t* tests or ANOVA and the Tukey test ($p < .05$) when comparing multiple groups. For “Single dilution per day” ALGiSIM campaigns, each data point represents the average and standard error for 8-daily replicates obtained from a single bioreactor campaign, except for STR30843, where two separate bioreactor campaigns were undertaken with 8-daily replicates measured for each run and an average and standard error was obtained. For the “Multiple dilution per day” experiments, each data point represents the average and standard error for two different ALGiSIM runs (biological replicates) with each replicate being sampled on 3–10 consecutive days ($n = 6–20$ total biomass measurements), with the exception of WT at 100% and 150% dilutions where only a single bioreactor campaign was undertaken with the 8–10 daily biomass measurements taken. Of the samples collected

over 3–10 days, 3–4 samples were used for photosynthetic measurements (each measured on the same day as harvest), 3–4 samples were used for pigment measurements, two samples were used for proteomic analysis, and one was used for TEM analysis.

AUTHOR CONTRIBUTIONS

Conception and design: AK, MC, SB, JV, FK, WL, JW, MP; collection and assembly of data: AK, MC, ML, CE; generation of strains STR30309 and STR30843: JV, MA; preliminary characterization for strain down selection: WL, FK, MN, YW, SB; analysis and interpretation of the data: AK, MC, TB, JW, MP; drafting of the article: AK, MC, JW, MP; critical revision: AK, MP, JW; final approval of the article: AK, MC, TB, DK, ML, SB, JV, WL, FK, MN, YW, CE, JW, MP, MA.

ACKNOWLEDGMENTS

This work was financially supported by ExxonMobil Technology and Engineering Company, United States. Electron microscopy sample preparation and imaging was done at the University of Colorado, Boulder EM Services Core Facility in the MCDB Department, with the technical assistance of facility staff in particular Garry P. Morgan and Dr. Eileen O’Toole. Proteomics sample preparation and quantification was done at Mass Spectrometry facility at University of Colorado Boulder, and Dr. Christopher Ebmeier was supported by S10 grant number S10OD025267. Authors would like to thank Dr. Eric Moellering, Dr. Edward Dempsey, Arron Harms, and Amy Ashford for their extensive support.

CONFLICT OF INTEREST STATEMENT

JCW and ML are employees of ExxonMobil, and research at the Colorado School of Mines was supported by an academic research grant from ExxonMobil.

PEER REVIEW

The peer review history for this article is available in the [Supporting Information](#) of this article.

DATA AVAILABILITY STATEMENT

Data available within the article or its supplementary materials.

ORCID

Anagha Krishnan  <https://orcid.org/0000-0002-0044-271X>

Devin A. Karns  <https://orcid.org/0000-0002-9360-5329>

Christopher C. Ebmeier  <https://orcid.org/0000-0001-7940-6190>

Joseph C. Weissman  <https://orcid.org/0000-0002-6278-4280>

Matthew C. Posewitz  <https://orcid.org/0000-0002-1163-8611>

REFERENCES

- Ajjawi, I., Verruto, J., Aqai, M., Soriaga, L. B., Coppersmith, J., Kwok, K., Peach, L., Orchard, E., Kalb, R., Xu, W. D., Carlson, T. J., Francis, K., Konigsfeld, K., Bartalis, J., Schultz, A., Lambert, W., Schwartz, A. S., Brown, R., & Moellering, E. R. (2017). Lipid production in *Nannochloropsis gaditana* is doubled by decreasing expression of a single transcriptional regulator. *Nature Biotechnology*, 35, 647–+. <https://doi.org/10.1038/nbt.3865>



- Amin, P., Sy, D. A., Pilgrim, M. L., Parry, D. H., Nussaume, L., & Hoffman, N. E. (1999). Arabidopsis mutants lacking the 43-and 54-kilodalton subunits of the chloroplast signal recognition particle have distinct phenotypes. *Plant Physiology*, 121, 61–70. <https://doi.org/10.1104/pp.121.1.61>
- Asakura, Y., Hirohashi, T., Kikuchi, S., Belcher, S., Osborne, E., Yano, S., Terashima, I., Barkan, A., & Nakai, M. (2004). Maize mutants lacking chloroplast FtsY exhibit pleiotropic defects in the biogenesis of thylakoid membranes[W]. *The Plant Cell*, 16, 201–214. <https://doi.org/10.1105/tpc.014787>
- Baek, K., Kim, D. H., Jeong, J., Sim, S. J., Melis, A., Kim, J.-S., Jin, E., & Bae, S. (2016). DNA-free two-gene knockout in *Chlamydomonas reinhardtii* via CRISPR-Cas9 ribonucleoproteins. *Scientific Reports*, 6, 30620. <https://doi.org/10.1038/srep30620>
- Barten, R. J. P., Wijffels, R. H., & Barbosa, M. J. (2020). Bioprospecting and characterization of temperature tolerant microalgae from Bonaire. *Algal Research*, 50, 102008. <https://doi.org/10.1016/j.algal.2020.102008>
- Becker, S. A., Spreafico, R., Kit, J. L., Brown, R., Likhogrud, M., Fang, W., Posewitz, M. C., Weissman, J. C., & Radakovits, R. (2020). Phased diploid genome sequence for the fast-growing microalga *Picochlorum celeri*. *Microbiology Resource Announcements*, 9(20), e00087-20. <https://doi.org/10.1128/MRA.00087-20>
- Beckmann, J., Lehr, F., Finazzi, G., Hankamer, B., Posten, C., Wobbe, L., & Kruse, O. (2009). Improvement of light to biomass conversion by deregulation of light-harvesting protein translation in *Chlamydomonas reinhardtii*. *Journal of Biotechnology*, 142, 70–77. <https://doi.org/10.1016/j.jbiotec.2009.02.015>
- Benedetti, M., Vecchi, V., Barera, S., & Dall'Osto, L. (2018). Biomass from microalgae: The potential of domestication towards sustainable bio-factories. *Microbial Cell Factories*, 17, 173. <https://doi.org/10.1186/s12934-018-1019-3>
- Bujaldon, S., Kodama, N., Rathod, M. K., Tourasse, N., Ozawa, S.-I., Sellés, J., Vallon, O., Takahashi, Y., & Wollman, F.-A. (2020). The BF4 and p71 antenna mutants from *Chlamydomonas reinhardtii*. *Biochimica et Biophysica Acta (BBA) - Bioenergetics* 1861, 148085, 1861, 148085. <https://doi.org/10.1016/j.bbabi.2019.148085>
- Cano, M., Karns, D. A. J., Weissman, J. C., Heinnickel, M. L., & Posewitz, M. C. (2021). Pigment modulation in response to irradiance intensity in the fast-growing alga *Picochlorum celeri*. *Algal Research*, 58, 102370. <https://doi.org/10.1016/j.algal.2021.102370>
- Cazzaniga, S., Dall'Osto, L., Szaub, J., Scibilia, L., Ballottari, M., Purton, S., & Bassi, R. (2014). Domestication of the green alga *Chlorella sorokiniana*: Reduction of antenna size improves light-use efficiency in a photobioreactor. *Biotechnology for Biofuels*, 7, 1, 157–163. <https://doi.org/10.1186/s13068-014-0157-z>
- Cook, P. M. (1951). Chemical engineering problems in large scale culture of algae. *Industrial and Engineering Chemistry*, 43, 2385–2389. <https://doi.org/10.1021/ie50502a056>
- Dabes, J. N., Wilke, C. R., & Sauer, K. H. (1970). *Microalgae for biofuels and animal feeds: Behavior of Chlorella pyrenoidosa in steady state continuous culture*. Department of energy.
- Dahlin, L. R., Gerritsen, A. T., Henard, C. A., van Wycken, S., Linger, J. G., Kunde, Y., Hovde, B. T., Starkenburg, S. R., Posewitz, M. C., & Guarnieri, M. T. (2019). Development of a high-productivity, halophilic, thermotolerant microalga *Picochlorum renovo*. *Communications Biology*, 2, 388. <https://doi.org/10.1038/s42003-019-0620-2>
- Davis, R., Aden, A., & Pienkos, P. T. (2011). Techno-economic analysis of autotrophic microalgae for fuel production. *Applied Energy*, 88, 3524–3531. <https://doi.org/10.1016/j.apenergy.2011.04.018>
- Dismukes, G. C., Carrieri, D., Bennette, N., Ananyev, G. M., & Posewitz, M. C. (2008). Aquatic phototrophs: Efficient alternatives to land-based crops for biofuels. *Current Opinion in Biotechnology*, 19, 235–240. <https://doi.org/10.1016/j.copbio.2008.05.007>
- Eppley, R. W., & Dyer, D. L. (1965). Predicting production in light-limited continuous cultures of algae. *Applied Microbiology*, 13, 833–837. <https://doi.org/10.1128/am.13.6.833-837.1965>
- Falk, S., & Sinning, I. (2010). cpSRP43 is a novel chaperone specific for light-harvesting chlorophyll a-b-binding proteins. *The Journal of Biological Chemistry*, 285, 21655–21661. <https://doi.org/10.1074/jbc.C110.132746>
- Foflonker, F., Ananyev, G., Qiu, H., Morrison, A., Palenik, B., Dismukes, G. C., & Bhattacharya, D. (2016). The unexpected extremophile: Tolerance to fluctuating salinity in the green alga *Picochlorum*. *Algal Research*, 16, 465–472. <https://doi.org/10.1016/j.algal.2016.04.003>
- Formighieri, C., Franck, F., & Bassi, R. (2012). Regulation of the pigment optical density of an algal cell: Filling the gap between photosynthetic productivity in the laboratory and in mass culture. *Journal of Biotechnology*, 162, 115–123. <https://doi.org/10.1016/j.jbiotec.2012.02.021>
- Friedland, N., Negi, S., Vinogradova-Shah, T., Wu, G., Ma, L., Flynn, S. P., Kumssa, T. T., Lee, C.-H., & Sayre, R. (2019). Fine-tuning the photosynthetic light harvesting apparatus for improved photosynthetic efficiency and biomass yield. *Scientific Reports*, 9, 13028. <https://doi.org/10.1038/s41598-019-49545-8>
- Giddings, T. H. Jr., Morpheus, M. K., & McIntosh, J. R. (2017). Preparing fission yeast for electron microscopy. *Cold Spring Harbor Protocols*, 2017(1). <https://doi.org/10.1101/pdb.prot091314>
- Gimpel, J. A., Specht, E. A., Georgianna, D. R., & Mayfield, S. P. (2013). Advances in microalgae engineering and synthetic biology applications for biofuel production. *Current Opinion in Chemical Biology*, 17, 489–495. <https://doi.org/10.1016/j.cbpa.2013.03.038>
- Gons, H., & Mur, L. (1975). An energy balance for algal populations in light-limiting conditions: With 2 figures in the text. *Internationale Vereinigung für Theoretische Und Angewandte Limnologie: Verhandlungen*, 19, 2729–2733.
- Gonzalez-Esquer, C. R., Wright, K. T., Sudasinghe, N., Carr, C. K., Sanders, C. K., Turmo, A., Kerfeld, C. A., Twary, S., & Dale, T. (2019). Demonstration of the potential of *Picochlorum soloecismus* as a microalgal platform for the production of renewable fuels. *Algal Research*, 43, 101658. <https://doi.org/10.1016/j.algal.2019.101658>
- Grobbelaar, J. U. (2000). Physiological and technological considerations for optimising mass algal cultures. *Journal of Applied Phycology*, 12, 201–206. <https://doi.org/10.1023/A:1008155125844>
- Grobbelaar, J. U. (2010). Microalgal biomass production: Challenges and realities. *Photosynthesis Research*, 106, 135–144. <https://doi.org/10.1007/s11120-010-9573-5>
- Grobbelaar, J. U., Nedbal, L., Tichy, L., & Setlik, L. (1995). Variation in some photosynthetic characteristics of microalgae cultured in outdoor thin-layered sloping reactors. *Journal of Applied Phycology*, 7, 175–184. <https://doi.org/10.1007/BF00693065>
- Grossman, A. R., Bhaya, D., Apt, K. E., & Kehoe, D. M. (1995). Light-harvesting complexes in oxygenic photosynthesis: Diversity, control, and evolution. *Annual Review of Genetics*, 29, 231–288. <https://doi.org/10.1146/annurev.ge.29.120195.001311>
- Henley, W. J., Hironaka, J. L., Guillou, L., Buchheim, M. A., Buchheim, J. A., Fawley, M. W., & Fawley, K. P. (2004). Phylogenetic analysis of the ‘Nannochloris-like’ algae and diagnoses of *Picochlorum oklahomensis* gen. et sp. nov. (Trebouxiophyceae, Chlorophyta). *Phycologia*, 43, 641–652. <https://doi.org/10.2216/i0031-8884-43-6-641.1>
- Huesemann, M. H., Hausmann, T. S., Bartha, R., Aksoy, M., Weissman, J. C., & Benemann, J. R. (2009). Biomass productivities in wild type and pigment mutant of *Cyclotella* sp. (diatom). *Applied Biochemistry and Biotechnology*, 157, 507–526. <https://doi.org/10.1007/s12010-008-8298-9>
- Hughes, C. S., Foehr, S., Garfield, D. A., Furlong, E. E., Steinmetz, L. M., & Krijgsveld, J. (2014). Ultrasensitive proteome analysis using paramagnetic bead technology. *Molecular Systems Biology*, 10(10), 757. <https://doi.org/10.15252/msb.20145625>

- Jansson, S., Pichersky, E., Bassi, R., Green, B. R., Ikeuchi, M., Melis, A., Simpson, D. J., Spangfort, M., Staehelin, L. A., & Thornber, J. P. (1992). A nomenclature for the genes encoding the chlorophylla/b-binding proteins of higher plants. *Plant Molecular Biology Reporter*, 10, 242–253. <https://doi.org/10.1007/BF02668357>
- Jeong, J., Baek, K., Kirst, H., Melis, A., & Jin, E. (2017). Loss of CpSRP54 function leads to a truncated light-harvesting antenna size in *Chlamydomonas reinhardtii*. *Biochimica et Biophysica Acta (BBA) - Bioenergetics*, 1858, 45–55. <https://doi.org/10.1016/j.bbabi.2016.10.007>
- Kirst, H., Formighieri, C., & Melis, A. (2014). Maximizing photosynthetic efficiency and culture productivity in cyanobacteria upon minimizing the phycobilisome light-harvesting antenna size. *Biochimica et Biophysica Acta-Bioenergetics*, 1837, 1653–1664. <https://doi.org/10.1016/j.bbabi.2014.07.009>
- Kirst, H., Gabilly, S. T., Niyogi, K. K., Lemaux, P. G., & Melis, A. (2017). Photosynthetic antenna engineering to improve crop yields. *Planta*, 245, 1009–1020. <https://doi.org/10.1007/s00425-017-2659-y>
- Kirst, H., García-Cerdán, J. G., Zurbriggen, A., & Melis, A. (2012). Assembly of the light-harvesting chlorophyll antenna in the green alga *Chlamydomonas reinhardtii* requires expression of the TLA2-CpFTSY gene. *Plant Physiology*, 158, 930–945. <https://doi.org/10.1104/pp.111.189910>
- Kirst, H., Garcia-Cerdan, J. G., Zurbriggen, A., Ruehle, T., & Melis, A. (2012). Truncated photosystem chlorophyll antenna size in the green microalga *Chlamydomonas reinhardtii* upon deletion of the TLA3-CpSRP43 gene. *Plant Physiology*, 160, 2251–2260. <https://doi.org/10.1104/pp.112.206672>
- Kirst, H., & Melis, A. (2014). The chloroplast signal recognition particle (CpSRP) pathway as a tool to minimize chlorophyll antenna size and maximize photosynthetic productivity. *Biotechnology Advances*, 32, 66–72. <https://doi.org/10.1016/j.biotechadv.2013.08.018>
- Kirst, H., Shen, Y., Vamvaka, E., Betterle, N., Xu, D., Warek, U., Strickland, J. A., & Melis, A. (2018). Downregulation of the CpSRP43 gene expression confers a truncated light-harvesting antenna (TLA) and enhances biomass and leaf-to-stem ratio in *Nicotiana tabacum* canopies. *Planta*, 248, 139–154. <https://doi.org/10.1007/s00425-018-2889-7>
- Klimyuk, V. I., Persello-Cartieaux, F., Havaux, M., Contard-David, P., Schuenemann, D., Meierhoff, K., Gouet, P., Jones, J. D., Hoffman, N. E., & Nussaume, L. (1999). A chromodomain protein encoded by the Arabidopsis CAO gene is a plant-specific component of the chloroplast signal recognition particle pathway that is involved in LHCP targeting. *The Plant Cell*, 11, 87–99. <https://doi.org/10.1105/tpc.11.1.87>
- Krishnan, A., Cano, M., Burch, T. A., Weissman, J. C., & Posewitz, M. C. (2020). Genome editing using Cas9-RNA ribonucleoprotein complexes in the high-productivity marine alga *Picochlorum celeri*. *Algal Research*, 49, 101944. <https://doi.org/10.1016/j.algal.2020.101944>
- Krishnan, A., Likhogrud, M., Cano, M., Edmundson, S., Melanson, J. B., Huesemann, M., McGowen, J., Weissman, J. C., & Posewitz, M. C. (2021). *Picochlorum celeri* as a model system for robust outdoor algal growth in seawater. *Scientific Reports*, 11, 11649. <https://doi.org/10.1038/s41598-021-91106-5>
- Kuzminov, F., Naghipor, M., Aqui, M., Wang, Y., & Verruto, J. (2022). *Chlorophyte algae having improved productivity Pending*, ed. (U.S. Patent Application #20220348946).
- Kwon, J.-H., Bernát, G., Wagner, H., Rögner, M., & Rexroth, S. (2013). Reduced light-harvesting antenna: Consequences on cyanobacterial metabolism and photosynthetic productivity. *Algal Research*, 2, 188–195. <https://doi.org/10.1016/j.algal.2013.04.008>
- Lamb, J. J., Røkke, G., & Hohmann-Marriott, M. F. (2018). Chlorophyll fluorescence emission spectroscopy of oxygenic organisms at 77 K. *Photosynthetica*, 56, 105–124. <https://doi.org/10.1007/s11099-018-0791-y>
- LaPanse, A. J., Krishnan, A., & Posewitz, M. C. (2021). Adaptive laboratory evolution for algal strain improvement: Methodologies and applications. *Algal Research*, 53, 102122. <https://doi.org/10.1016/j.algal.2020.102122>
- Lee, Y.-K. (2001). Microalgal mass culture systems and methods: Their limitation and potential. *Journal of Applied Phycology*, 13, 307–315. <https://doi.org/10.1023/A:1017560006941>
- Macintyre, H., Kana, T., Anning, T., & Geider, R. (2002). Photoacclimation of photosynthesis irradiance response curves and photosynthetic pigments in microalgae and cyanobacteria 1. *Journal of Phycology*, 38, 17–38. <https://doi.org/10.1046/j.1529-8817.2002.00094.x>
- Manjre, S., Paul, K., Patil, S., Pai, P., Banerjee, A., Sarkar, P., Teredesai, A., Shukla, M. R., & Dasgupta, S. (2022). Evaluating the effect of seasonal conditions on metabolism and photosynthetic performance of *Picochlorum* sp. and its influence on biomass productivity. *Biore-source Technology Reports*, 18, 101029. <https://doi.org/10.1016/j.biteb.2022.101029>
- McAvoy, C. Z., Siegel, A., Piszkievicz, S., Miaou, E., Yu, M., Nguyen, T., Moradian, A., Sweredoski, M. J., Hess, S., & Shan, S. O. (2018). Two distinct sites of client protein interaction with the chaperone cpSRP43. *The Journal of Biological Chemistry*, 293, 8861–8873. <https://doi.org/10.1074/jbc.RA118.002215>
- Melis, A. (2009). Solar energy conversion efficiencies in photosynthesis: Minimizing the chlorophyll antennae to maximize efficiency. *Plant Science*, 177, 272–280. <https://doi.org/10.1016/j.plantsci.2009.06.005>
- Melis, A., Neidhardt, J., & Benemann, J. R. (1998). *Dunaliella salina* (Chlorophyta) with small chlorophyll antenna sizes exhibit higher photosynthetic productivities and photon use efficiencies than normally pigmented cells. *Journal of Applied Phycology*, 10, 515–525. <https://doi.org/10.1023/A:1008076231267>
- Mitra, M., Kirst, H., Dewez, D., & Melis, A. (2012). Modulation of the light-harvesting chlorophyll antenna size in *Chlamydomonas reinhardtii* by TLA1 gene over-expression and RNA interference. *Philosophical Transactions of the Royal Society of London. Series B, Biological Sciences*, 367, 3430–3443. <https://doi.org/10.1098/rstb.2012.0229>
- Moheimani, N. R., & Borowitzka, M. A. (2007). Limits to productivity of the alga *Pleurochrysis carterae* (Haptophyta) grown in outdoor raceway ponds. *Biotechnology and Bioengineering*, 96, 27–36. <https://doi.org/10.1002/bit.21169>
- Mussgnug, J. H., Thomas-Hall, S., Rupprecht, J., Foo, A., Klassen, V., McDowall, A., Schenk, P. M., Kruse, O., & Hankamer, B. (2007). Engineering photosynthetic light capture: Impacts on improved solar energy to biomass conversion. *Plant Biotechnology Journal*, 5, 802–814. <https://doi.org/10.1111/j.1467-7652.2007.00285.x>
- Mussgnug, J. H., Wobbe, L., Elles, I., Claus, C., Hamilton, M., Fink, A., Kahmann, U., Kapazoglou, A., Mullineaux, C. W., Hippler, M., Nickelsen, J., Nixon, P. J., & Kruse, O. (2005). NAB1 is an RNA binding protein involved in the light-regulated differential expression of the light-harvesting antenna of *Chlamydomonas reinhardtii*. *Plant Cell*, 17, 3409–3421. <https://doi.org/10.1105/tpc.105.035774>
- Myers, J., & Graham, J. R. (1959). On the mass culture of algae. II. Yield as a function of cell concentration under continuous sunlight irradiance. *Plant Physiology*, 34(3), 345–352. <https://doi.org/10.1104/pp.34.3.345>
- Nakajima, Y., Tsuzuki, M., & Ueda, R. (2001). Improved productivity by reduction of the content of light-harvesting pigment in *Chlamydomonas perigranulata*. *Journal of Applied Phycology*, 13, 95–101. <https://doi.org/10.1023/A:1011192832502>
- Nakajima, Y., & Ueda, R. (2000). The effect of reducing light-harvesting pigment on marine microalgal productivity. *Journal of Applied Phycology*, 12, 285–290. <https://doi.org/10.1023/A:1008108500409>
- Negi, S., Perrine, Z., Friedland, N., Kumar, A., Tokutsu, R., Minagawa, J., Berg, H., Barry, A. N., Govindjee, G., & Sayre, R. (2020). Light



- regulation of light-harvesting antenna size substantially enhances photosynthetic efficiency and biomass yield in green algae(†). *The Plant Journal*, 103, 584–603. <https://doi.org/10.1111/tpj.14751>
- Nymark, M., Volpe, C., Hafskjold, M. C. G., Kirst, H., Serif, M., Vadstein, O., Bones, A. M., Melis, A., & Winge, P. (2019). Loss of ALBINO3b Insertase results in truncated light-harvesting antenna in diatoms. *Plant Physiology*, 181, 1257–1276. <https://doi.org/10.1104/pp.19.00868>
- Oey, M., Ross, I. L., Stephens, E., Steinbeck, J., Wolf, J., Radzun, K. A., Kügler, J., Ringsmuth, A. K., Kruse, O., & Hankamer, B. (2013). RNAi knock-down of LHCBM1, 2 and 3 increases photosynthetic H₂ production efficiency of the green alga *Chlamydomonas reinhardtii*. *PLoS ONE*, 8, e61375. <https://doi.org/10.1371/journal.pone.0061375>
- Perin, G., Bellan, A., Segalla, A., Meneghesso, A., Alborese, A., & Morosinotto, T. (2015). Generation of random mutants to improve light-use efficiency of *Nannochloropsis gaditana* cultures for biofuel production. *Biotechnology for Biofuels*, 8, 161. <https://doi.org/10.1186/s13068-015-0337-5>
- Perrine, Z., Negi, S., & Sayre, R. T. (2012). Optimization of photosynthetic light energy utilization by microalgae. *Algal Research*, 1, 134–142. <https://doi.org/10.1016/j.algal.2012.07.002>
- Pirt, J. S. (1986). The thermodynamic efficiency (quantum demand) and dynamics of photosynthetic growth. *New Phytologist*, 102, 3–37. <https://doi.org/10.1111/j.1469-8137.1986.tb00794.x>
- Polle, J. E., Benemann, J. R., Tanaka, A., & Melis, A. (2000). Photosynthetic apparatus organization and function in the wild type and a chlorophyll b-less mutant of *Chlamydomonas reinhardtii*. Dependence on carbon source. *Planta*, 211, 335–344.
- Polle, J. E., Kanakagiri, S. D., & Melis, A. (2003). tla1, a DNA insertional transformant of the green alga *Chlamydomonas reinhardtii* with a truncated light-harvesting chlorophyll antenna size. *Planta*, 217, 49–59. <https://doi.org/10.1007/s00425-002-0968-1>
- Qin, X., Suga, M., Kuang, T., & Shen, J.-R. (2015). Structural basis for energy transfer pathways in the plant PSI-LHCI supercomplex. *Science*, 348, 989–995. <https://doi.org/10.1126/science.aab0214>
- Radmer, R., & Kok, B. (1977). Photosynthesis: Limited yields, unlimited dreams. *Bioscience*, 27, 599–605. <https://doi.org/10.2307/1297655>
- Schenk, P. M., Thomas-Hall, S. R., Stephens, E., Marx, U. C., Mussgnug, J. H., Posten, C., Kruse, O., & Hankamer, B. (2008). Second generation biofuels: High-efficiency microalgae for biodiesel production. *Bioenergy Research*, 1, 20–43. <https://doi.org/10.1007/s12155-008-9008-8>
- Schwede, T., Kopp, J., Guex, N., & Peitsch, M. C. (2003). SWISS-MODEL: An automated protein homology-modeling server. *Nucleic Acids Research*, 31, 3381–3385. <https://doi.org/10.1093/nar/gkg520>
- Sheehan, J., Dunahay, T., Benemann, J., & Roessler, P. (1998). A Look Back at the U.S. Department of Energy's Aquatic Species Program—Biodiesel from Algae. Golden, CO (United States): National Renewable Energy Lab. (NREL). <https://doi.org/10.2172/15003040>
- Shin, W.-S., Lee, B., Jeong, B.-R., Chang, Y. K., & Kwon, J.-H. (2016). Truncated light-harvesting chlorophyll antenna size in *Chlorella vulgaris* improves biomass productivity. *Journal of Applied Phycology*, 28, 3193–3202. <https://doi.org/10.1007/s10811-016-0874-8>
- Stengel, K. F., Holdermann, I., Cain, P., Robinson, C., Wild, K., & Sinning, I. (2008). Structural basis for specific substrate recognition by the chloroplast signal recognition particle protein cpSRP43. *Science*, 321, 253–256. <https://doi.org/10.1126/science.1158640>
- Su, X., Ma, J., Wei, X., Cao, P., Zhu, D., Chang, W., Liu, Z., Zhang, X., & Li, M. (2017). Structure and assembly mechanism of plant C2S2M2-type PSII-LHCII supercomplex. *Science*, 357, 815–820. <https://doi.org/10.1126/science.aan0327>
- Wang, P., Liang, F. C., Wittmann, D., Siegel, A., Shan, S. O., & Grimm, B. (2018). Chloroplast SRP43 acts as a chaperone for glutamyl-tRNA reductase, the rate-limiting enzyme in tetrapyrrole biosynthesis. *Proceedings of the National Academy of Sciences of the United States of America*, 115, E3588–e3596. <https://doi.org/10.1073/pnas.1719645115>
- Weissman, J. C. (1978). *Bioconversion of Solar Energy*. University of California Berkeley.
- Weissman, J. C., & Benemann, J. R. (1979). Biomass recycling and species competition in continuous cultures. *Biotechnology and Bioengineering*, 21, 627–648. <https://doi.org/10.1002/bit.260210408>
- Weissman, J. C., Likhogrud, M., Thomas, D. C., Fang, W., Karns, D. A. J., Chung, J. W., Nielsen, R., & Posewitz, M. C. (2018). High-light selection produces a fast-growing *Picochlorum celeri*. *Algal Research*, 36, 17–28. <https://doi.org/10.1016/j.algal.2018.09.024>
- Weissman, J., & Nielsen, R. (2016). *Algal Growth Kinetics and Productivity* (pp. 21–62). CRC Press.
- Ziehe, D., Dünschede, B., & Schünemann, D. (2018). Molecular mechanism of SRP-dependent light-harvesting protein transport to the thylakoid membrane in plants. *Photosynthesis Research*, 138, 303–313. <https://doi.org/10.1007/s11120-018-0544-6>

SUPPORTING INFORMATION

Additional supporting information can be found online in the Supporting Information section at the end of this article.

How to cite this article: Krishnan, A., Cano, M., Karns, D. A., Burch, T. A., Likhogrud, M., Aqai, M., Bailey, S., Verruto, J., Lambert, W., Kuzminov, F., Naghipor, M., Wang, Y., Ebmeier, C. C., Weissman, J. C., & Posewitz, M. C. (2023). Simultaneous CAS9 editing of cpSRP43, LHCA6, and LHCA7 in *Picochlorum celeri* lowers chlorophyll levels and improves biomass productivity. *Plant Direct*, 7(9), e530. <https://doi.org/10.1002/pld3.530>